Development of a Microfluidic System for Separation, Aggregation and Nanocrystallization of Effector Proteins

Master's Thesis

written by
Jan Burri

supervised by
Stefan Arnold
(C-CINA, University of Basel)

submitted to
Dr. Thomas Braun
Prof. Dr. Henning Stahlberg
(C-CINA, University of Basel)

Biozentrum
University of Basel

31.01.2015

UNIVERSITÄT BASEL

PHILOSOPHISCH-NATURWISSENSCHAFTLICHE FAKULTÄT

Erklärung zur wissenschaftlichen Redlichkeit
(beinhaltet Erklärung zu Plagiat und Betrug)

Bachelorarbeit / Masterarbeit *(nicht Zutreffendes bitte streichen)*

Titel der Arbeit *(Druckschrift)*:

Development of a Microfluidic System for Separation, Aggregation and Nanocrystallization of Effector Proteins

Name, Vorname *(Druckschrift)*: Burri, Jan

Matrikelnummer: 09-058-512

Hiermit erkläre ich, dass mir bei der Abfassung dieser Arbeit nur die darin angegebene Hilfe zuteil wurde und dass ich sie nur mit den in der Arbeit angegebenen Hilfsmitteln verfasst habe.

Ich habe sämtliche verwendeten Quellen erwähnt und gemäss anerkannten wissenschaftlichen Regeln zitiert.

Diese Erklärung wird ergänzt durch eine separat abgeschlossene Vereinbarung bezüglich der Veröffentlichung oder öffentlichen Zugänglichkeit dieser Arbeit.

☒ ja ☐ nein

Ort, Datum: Basel, 31.01.2015

Unterschrift:

Dieses Blatt ist in die Bachelor-, resp. Masterarbeit einzufügen.

UNI BASEL

Abstract

Many neurodegenerative diseases are linked to protein aggregation. Endogenous proteins misfold and assemble into insoluble fibrous structures, called amyloids, which are associated with neuronal degradation. This misfolding can be imprinted onto healthy protein, leading to a progressive and stereotypic spreading of the aggregation throughout the affected brain. Interestingly, new reports suggest that these amyloidogenic proteins such as α-synuclein of the Parkinson's disease, can adopt distinct structures, forming aggregates differing in toxicity and seeding properties. However, the pathomechanism of the spreading is unknown, as well as the mechanism of the pathogenesis leading to the initial amyloids.

This thesis focuses on the aggregation process of amyloids and the search of effector substances (proteins) leading to aggregation. To this end, microfluidic systems were developed for (i) studying the aggregation process upon the mixing of amyloidogenic proteins with effector proteins and (ii) separation of complex mixtures to isolate potential effector proteins for testing in a new aggregation chip.

For the seeding and aggregation experiments, a previously described two-phase microcrystallization setup with a 3+1 mixer was implemented. The aggregation processes were monitored using birefringence, UV imaging and SONICC. The created aggregates can be later used for structural *ex situ* analysis applying cryo-EM. The ultimate goal is to obtain a library of different aggregate structures with atomic resolution and the corresponding pathology.

A capillary zone electrophoresis setup was established to separate effector proteins from complex mixtures. A test sample consisting of lysozyme and RNase was successfully separated using K_2SO_4 in HEPES at pH 7.4. Furthermore first separation experiments with HEK cell lysate were made. In the future, the capillary zone electrophoresis setup and the aggregation platform can be combined to search for potential effectors inducing amyloid aggregation.

Keywords: neurodegenerative diseases, α-synuclein, aggregation, nanocrystallization, capillary zone electrophoresis, two-phase microfluid

Contents

1 Introduction

Neurodegenerative diseases affect the nervous system and leads to nerve cell degeneration. Usually these diseases slowly progress, often resulting in dementia and movement disorders. Most of these diseases are associated with aggregation of specific proteins in the human brain. The aggregation is a result of misfolded proteins, such as amyloid-β (Aβ) and tau in Alzheimer's disease (AD), α-synuclein (αS) in Parkinson's disease (PD), huntingtin (Htt) in Huntington's disease (HD) and the normal conformer prion protein (PrP^C) in prion diseases [Costanzo & Zurzolo 2013]. Therefore these diseases are referred to as protein misfolding disorders (PMD). Although the proteins have different tertiary, mostly unfolded, structures, they aggregate into similar insoluble fibrous structures with ordered arrangement of β-sheets, called amyloids [Sunde *et al.* 1997]. In this thesis a method is presented to separate amyloidogenic proteins and to study their influence on protein aggregation.

Contents

1.1 Aggregation of Proteins in Neurodegenerative Diseases

1.1.1 Prion Diseases

Among the PMD, the prion diseases have to be treated differently, since they are the only ones which are verifiably infectious between different individuals and even across species [Aguzzi & Calella 2009]. The trigger for a prion disease is a misfolded protein (pathogenic prion protein conformer PrP^{Sc}), which can occur spontaneously or has originated from an exogenous source. The PrP^{Sc} induces a conformation change in contact with the correctly folded PrP^C, which is then misfolded into a PrP^{Sc} as well. This transmission of the own misfolding onto another protein is called templated conformation change. This leads to a spreading and aggregation of the PrP^{Sc} across the affected brain [Aguzzi & Calella 2009]. The injection or intake of PrP^{Sc} from a exogenous source is referred to as seeding.

1.1.2 Prion-like Mechanism in Neurodegenerative Diseases

The other PMD have similar properties as the prion diseases, but it has to be highlighted that in comparison, there is no evidence of spontaneous infectivity. The first similarity is the spreading of the aggregates through the affected brain. Compared to the prions, these aggregates are too large to simply diffuse through the membranes. Therefore it is suggested that the disease is spread by an unknown cell-to-cell transfer of misfolded, aggregated proteins, which then leads to misfoldings in the new cell [Frost & Diamond 2010]. The second similarity is the wide diversity of different diseases triggered by the same protein. This indicates that a protein can aggregate into different structures, which leads to different pathologies. Because of these similarities the proteins are said to behave prion-like.

1.1.3 Aggregates of α-Synuclein

Because of the large heterogeneity of the neurodegenerative diseases and the difficult and unknown transport mechanism, it is crucial to first investigate the fundamental principles. Therefore the focus of this thesis will be mainly on αS aggregation and the diseases associated with it. Besides PD, this includes dementia with Lewy bodies and multiple-system atrophy [Goedert 2001]. One pathological feature of the so-called α-synucleinopathies are the Lewy bodies (LB), which are filamentous inclusion in nerve and glia cells [Goedert 2001]. These LBs consist mainly of aggregated αS [Spillantini *et al.* 1997]. Therefore the aggregation of αS needs further investigation. Native αS is a soluble unfolded monomer without well-defined secondary and tertiary structures [Weinreb *et al.* 1996]. It promotes SNARE formation in the presynaptic terminal and modulates synaptic functions [Burré *et al.* 2010]. The misfolded αS forms fibrils consisting mostly of β-sheets [Spillantini *et al.* 1997, Vilar *et al.* 2008] similar to other amyloidogenic proteins [Sunde *et al.* 1997]. Some evidence that the αS fibrils are in fact prion-like and misfolding is passed from a misfolded protein onto a native one is given by seeding experiments. [Waxman & Giasson 2010]. Furthermore cellular transfers were observed [Hansen *et al.* 2011]. This is strong evidence that αS amyloids can penetrate the cell membrane and spread into healthy cells. Even stronger evidence is given by *in vivo* experiments. It was shown that misfolded αS seeded into mice brains lead to further aggregations and even LB-like inclusions [Angot *et al.* 2012]. The areas around the injection points were first affected, whereas at later stages larger areas were involved. This indicates a spreading and a cell-to-cell transport of the misfolded αS. The exact mechanisms how the αS amyloids escape the cells and are ingested into healthy cells are still unclear. There are different proposals of the cell-to-cell transport [Frost & Diamond 2010, Costanzo & Zurzolo 2013] but without clear evidences. Interestingly, αS has been reported to form stable pore-like oligomeres

[Volles *et al.* 2001], which could be one way of entering or escaping a cell. In PMD patients often different types of amyloidogenic proteins are detected. This indicates that the formations of some amyloid are promoted or triggered by other amyloidogenic proteins, also called cross-seeding [Waxman & Giasson 2011, Guo *et al.* 2013].

Further, the cause of the large diversity of different pathologies has to be investigated. In prion diseases the large diversity arises from different structures of the aggregates which results in different properties. Therefore different diseases are developed [Ironside *et al.* 2005]. There are in fact different structures of αS aggregates. It was shown, that these polymorphs have different levels of toxicity, as well as different seeding and propagation properties [Bousset *et al.* 2013]. Furthermore there is evidence, that the structure influences the ability for cross-seeding other amyloidogenic proteins (e.g. tau) [Guo *et al.* 2013]. Importantly it has been shown, that the original conformation of the seeding protein is transmitted onto the native proteins, resulting in similar conformations [Yonetani *et al.* 2009].

The ultimate goal would be to have a library of the structures of different αS polymorphs with the corresponding synucleinopathy and the associated disease propagation.

1.2 Analysis of Aggregates and Nanocrystals

In this thesis a microfluidic pipeline (Figure 1) from protein separation (Figure 1A) to protein analysis (Figure 1C) is presented. A separation system is needed to separate the effector molecules from complex environments (e.g. cell lysate, brain tissue). Such a system was established during the master's thesis. Since the further analysis depends on aggregates and crystals, an additional step, a crystallization instrument, has to be integrated into the microfluidic pipeline (Figure 1B). This instrument can further be used to monitor the aggregation and crystallization processes. The microfluidic crystallization system presented in this thesis was previously discribed in [Burri 2014].

The aggregated nanocrystals can be used to determine the protein structures. Usually, this is done by the X-ray diffraction, where X-rays are fired onto a crystal, scattered at its lattice and the diffraction pattern is recorded. A set of diffraction patterns is obtained by exposing the crystal again at different slightly rotated positions. This set of diffraction images is used to derive the original structure of the protein lattice via Fourier transformation. Unfortunately, the X-ray radiation damages the sample via inelastic scattering, which only allows large crystals to be examined. Therefore nanocrystals have to be studied using other approaches. One approach is the use of the X-ray free-electron laser (XFEL) [Chapman *et al.* 2011, Bogan 2013], where a short pulsed laser hits a nanocrystal and diffracts before the high energy

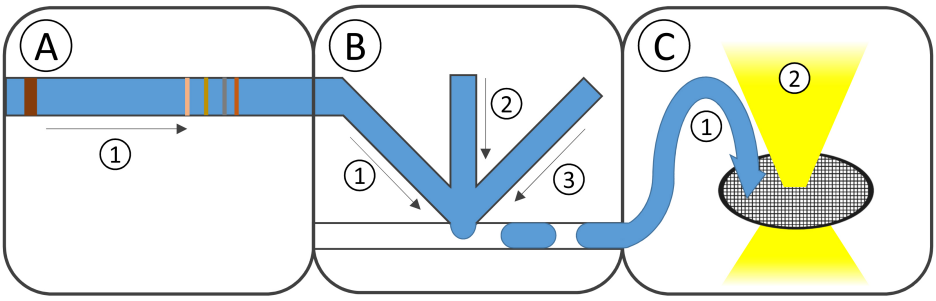

Figure 1: Microfluidic pipeline for studying protein aggregation and crystallization system consisting of three parts. (A) A separation system using capillary electrophoresis (1) to separate protein mixtures. (B) A two-phase micro-crystallization chip is used to mix the separated proteins (1) with buffer (2) and a third component (e.g. natively folded monomers, precipitant) (3) and form droplets separated by an immiscible phase. The droplets are then incubated and analysed *in situ*. (C) For the *ex situ* analyses of the droplets (2) a handover (1) is needed

vaporizes the crystal. The so-called diffraction before destruction offers diffraction images, free from damage induced disturbances [Doerr 2011]. Since the crystals are destroyed by the exposure, a large amount of nanocrystals is needed to create a series of diffraction patterns from different orientations.

The more promising approach is using electrons instead of photons, more precisely using a cryo-electronmicroscope (cryo-EM). First, in micro-electron-diffraction (MicroED) low energy electrons are used to diffract at nanocrystals under different orientations [Shi *et al.* 2013, Nederlof *et al.* 2013]. Second the use of direct electron detection (DED) cameras in cryo-EM allows the structure determination of large molecules by a single particle approach, without the use of crystals [Zhou 2008, Kühlbrandt & Williams 1999]. The single particle approach is very interesting, since it allows to analyse protein aggregation without crystalline structures as well.

1.3 Capillary Zone Electorphoresis (CZE)

Different separation methods such as size-exclusion chromatography, analytical ultracentrifugation and electrophoresis were already used for separating different aggregates of neurodegenerative effector proteins [Pedersen & Heegaard 2013]. The separation method used in this thesis is the capillary electrophoresis (CE), since it combines a simple setup with a good efficiency. CE was already used to monitor the concentration change of both, monomer and early state oligomere of Aβ [Pedersen *et al.* 2011]. The basic principles of CE were described in 1983 [Jorgenson & Lukacs 1983].

Since then, the setups were improved and adapted to different applications. This resulted in several modes to operate the CE. The different techniques range from capillary zone electrophores (CZE), which is used in our setup, to capillary isoelectric focusing [Rodriguez-Diaz *et al.* 1997], capillary gel electrophoresis [Dolník 1994], isotachophoresis [Malá *et al.* 2013] and micellar electrokinetik capillary chromatography.

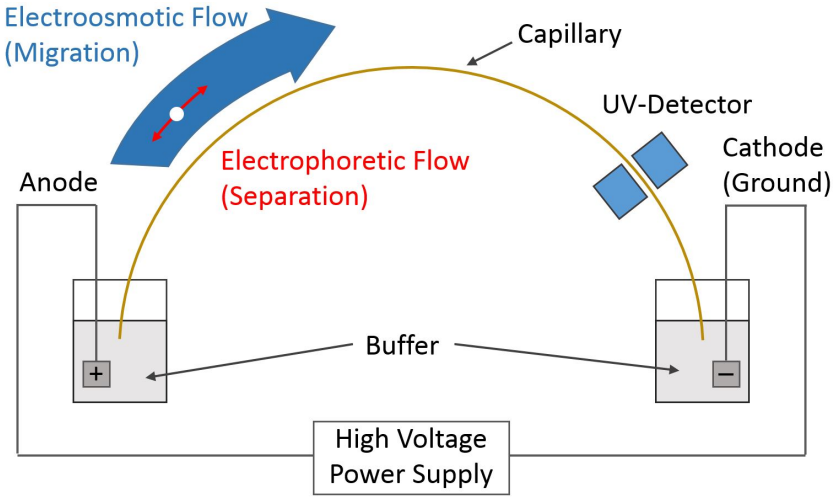

Figure 2: Schematic drawing of a capillary zone electrophoresis setup. A capillary is placed into two flasks, one with an anode and one with a cathode electrode. An applied high voltage (10 - 30 kV) leads to an electroosmotic flow and a electrophoretic separation. The separation of the proteins is monitored by a detector.

The CZE is a relatively simple method to perform high efficiency separation of large and small particles. The particles are separated by charge, size and shape. The setup (Figure 2) is simple. Each end of a narrow bore (ID = 25 - 75 µm) capillary is dipped into a flask filled with buffer. An anode electrode is placed into one of the flasks and a cathode (ground) electrode into the other. A controllable high voltage power supply provides a high voltage (10 - 30 kV) between the electrodes. The most complicated part is the capillary protein detector (CPD) which is used to monitor the separation and detect the different protein bands. After a sample is injected into the capillary, the high voltage is switched on and the separation starts. Two different flows arise from the electric field generated by the high voltage. The electroosmotic flow (EOF) leads to a propagation of the sample through the capillary whereas the electrophoretic migration separates the sample. The small bore of the capillary prevents a large Joule heating since the current is quite small and the large surface leads to an efficient cooling. Therefore high voltages can be applied without heating the sample which increases the efficiency of the separation.

1.3.1 Electroosmotic Flow (EOF)

The capillary consists of fused silica which has a isoelectric point of about 1.5. When the pH of the running buffer is above that value, the walls are negatively charged. The positively charged electrolytes of the buffer solution are attracted by the wall and an electric double layer is formed. This thin layer of positively charged electrolytes has a net charge, whereas the unordered bulk solution does not (Figure 3). When a voltage is applied, the positively charged layer moves towards the cathode, dragging the bulk solution with it. The generated flow through the cathode is the electroosmotic flow (EOF). The flow rate of this EOF is given by the following equation

$$v_{eo} = \frac{\epsilon\zeta}{4\pi\eta}E \tag{1}$$

where ϵ is the dielectric constant of the buffer and η its the viscosity. E is the electric field and ζ the zeta potential. The EOF is independent of the injected sample and only depends on the running buffer. The zeta potential arise at the liquid-solid interface and is related to the inverse of the square root concentration of the electrolyte. Therefore an increase of the electrolyte concentration decreases the EOF.

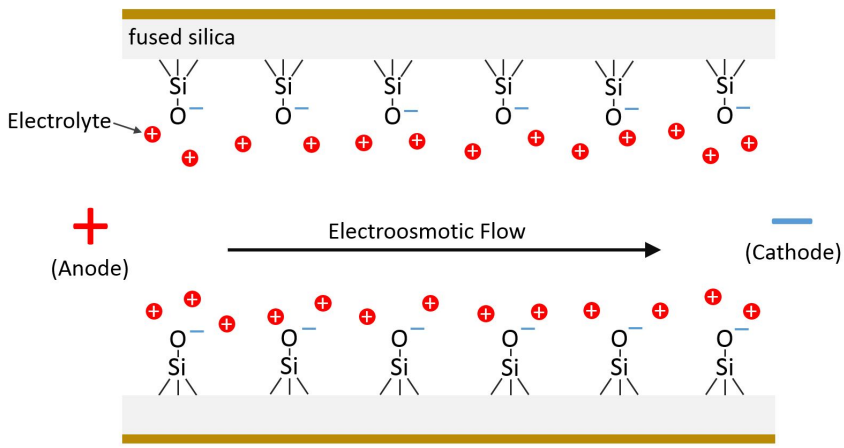

Figure 3: Negatively charged capillary walls attract positively charged electrolyte to form an electric double layer. The positively charged layer move towards the cathode and form the driving force of the EOF.

1.3.2 Flow Profile

The flow profile of a liquid pumped through a capillary, e.g. driven by hydrostatic pressure or by syringe pumps, is described by the laminar Poiseuille flow. This hydrodynamic flow (Figure 4A) has some unfortunate disadvantages. Due to the viscosity of the fluid, the flow rate of the liquid is zero at the walls. The flow rate then increases when approaching the centre of the capillary until it reaches its maximum. Since the liquid near the walls is slowed down and diffuse into the following components, the effective diffusion and mixing in flow direction is increased. This effect is called Taylor dispersion.

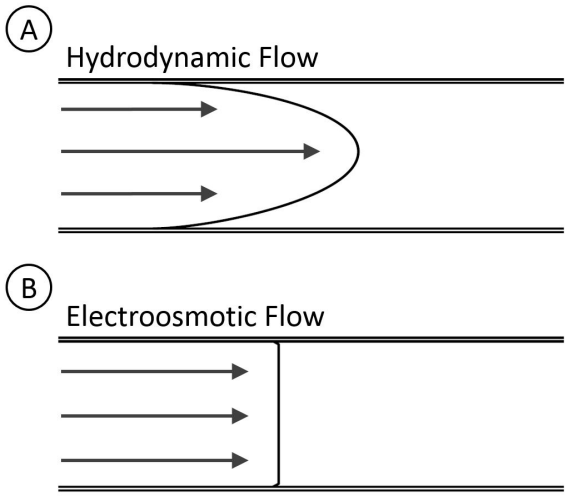

Figure 4: Comparison of the cross sectional flow profile of (A) the hydrodynamic and (B) the electroosmotic flow.

The Taylor dispersion is prevented in the CZE by the EOF. The homogeneous distributed electric double layer over the capillary leads to an uniform flow rate through the cross section of the capillary (Figure 4B). The flow rate reaches zero at the wall as well, but this effect occurs much later. This flow profile assures that the CZE can separate the protein mixtures into concrete bands which stay separated and do not mix during liquid transport through the capillary.

1.3.3 Electrophoretic Migration

The driving force of the separation is the electrophoretic migration. Positively and negatively charged particles are attracted by the cathode and the anode, respectively. Therefore they experiencing an acceleration towards the respective electrode, until an equilibrium with the velocity dependent friction is reached (Figure 5). Therefore

the CZE is a separation by charge, size and shape of the individual proteins.

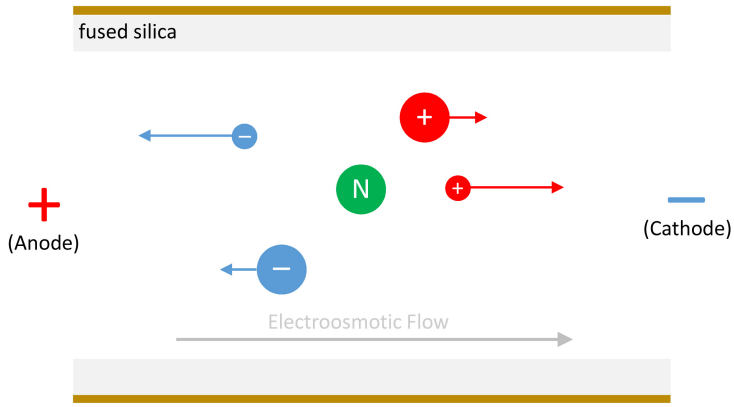

Figure 5: Electrophoretic migration describes the separation of particles by their charge, size and shape. Positively resp. negatively charged particles migrate towards the cathode resp. anode. Smaller particles move faster than larger particles.

The velocity of the electrophoretic migration is given by

$$v_{ep} = \mu_{ep} E = \frac{\epsilon \zeta}{4\pi\eta} E \tag{2}$$

where v_{ep} is the electrophoretic migration, μ_{ep} the electrophoretic mobility, ζ is the zeta potential, η is the viscosity of the buffer and E is the electric field. The equation can be approximated using the Debye-Hückel-Henry theory

$$v_{ep} = \mu_{ep} E = \frac{q}{6\pi\eta R} E \tag{3}$$

Here, the electrophoretic mobility μ_{ep} solely dependents on the charge q and the Stokes radius R of the migrating protein, and the viscosity of the buffer η.

1.3.4 Buffer and Additives

It is crucial to choose the right running buffer. The buffer is most effective within one or two pH units of its isoelectric point. Typical Buffer concentration used in CZE are between 50 - 100 mM. Zwitterionic buffers are often used since their low conductivity leads to a small current, which prevents Joule heating. Different buffers and the corresponding pH range, they are used in, are seen in Table 1.

Buffer	**Useful pH Range**
Phosphate	1.14 - 3.14
	6.20 - 8.20
Acetate	3.76 - 5.76
Borate	8.14 - 10.14
Zwitterionic Buffers	
MES	5.15 - 7.15
PIPES	5.80 - 7.80
HEPES	6.55 - 8.55
Tricine	7.15 - 9.15
Tris	7.30 - 9.30

Table 1: A small selection of different buffers and the typical used pH range.

Additives	**Function**
Inorganic salts	Protein conformational changes
Organic solvents	Solubilizer, modify electroosmotic flow
Urea	Solubilize and denature proteins
Sulfonic acids	Ion pairing agents, hydrophobic interaction agents
Cationic surfactants	Charge reversal of capillary wall
Cellulose derivatives	Reduce electroosmotic flow, provide a sieving medium
Amines	Cover free silanol groups

Table 2: Buffer additives can change the selectivity of the separation e.g. by altering the electrophoretic mobility of some proteins.

Additives can be added to the buffer to increase the resolution of the separation or to enable separation of otherwise inseparable proteins. Additives can alter, among other things, the electrophoretic mobilities of the proteins. The effect of different additives can be seen in Table 2. There is no general rule which additive to use when. The right additive for a each separation has to be found empirically.

1.4 Microcapillary Protein Crystallization System (MPCS)

The microcapillary protein crystallization system (MPCS) consists of three inlets with aqueous components and one with an immiscible carrier fluid (e.g. mcs-oil 04 (20-5004-0000-00, microfluidic ChipShop)). These four inlets merge into one microchannel and form the so called 3+1 mixer (Figure 6A). At this point the components mix and form droplets (15 - 20 nl) in the carrier fluid. This allows hundreds of individual experiments in these droplets with slightly different chemical compositions. Up to 400 droplets can be generated and stored in a microchannel circuit for incubation (Figure 6B). The MPCS allows to analyse rare and expensive samples, since it requires only very small sample volumes.

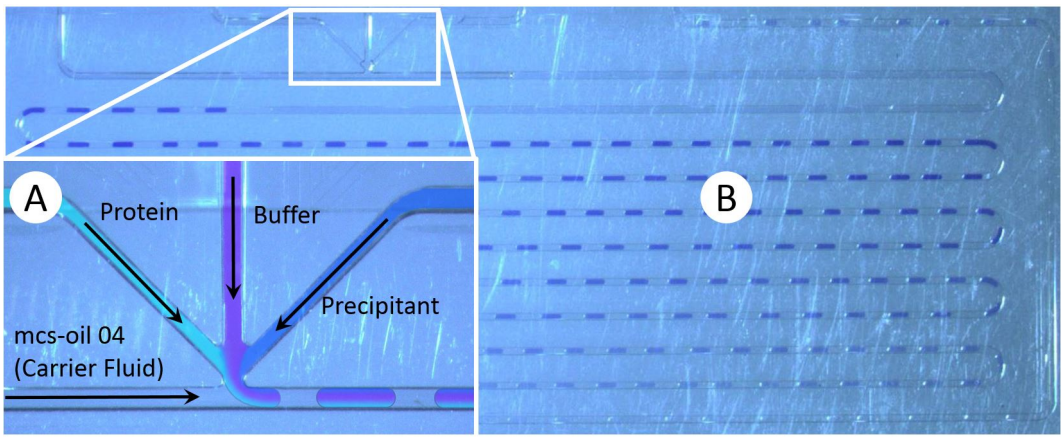

Figure 6: The three aqueous components are mixed at the 3+1 mixer and form droplets in the carrier fluid (a). The droplets are then stored for incubation (b).

1.4.1 Concentration Gradient

The different chemical compositions in the droplets are obtained by varying the concentration of the three aqueous components. This is done by adjusting the individual flow rates of each inlet. The relative flow rates define the concentration of

each component in the droplets. The summed flow rate of the inlets and the carrier fluid flow rate can be used to tune the droplet sizes. During the experiment, these are held constant to guarantee droplets of similar size and volume.

1.4.2 Protein Crystallization and Aggregation

For the crystallization, buffer, precipitant and protein solution are used as the aqueous components. The MPCS allows a fine tuning of the precipitant and protein concentration to optimize the crystallization conditions [Gerdts *et al.* 2010]. The goal is to reach the condition in which the proteins start to nucleate and therefore form nano- and microcrystals. Two simple approaches to achieve this are shown in Figure 7. In both approaches the precipitant concentration is increased. The protein concentration is either held constant (Figure 7A) or simultaneously decreased (Figure 7B). The buffer flow rate is adjusted in such a way, that the overall flow rate is constant. Since the crystallization conditions must be more or less known, the MPCS does not replace previous high throughput screenings to find the crystallization condition, but might assist to increase the quality of the protein crystals.

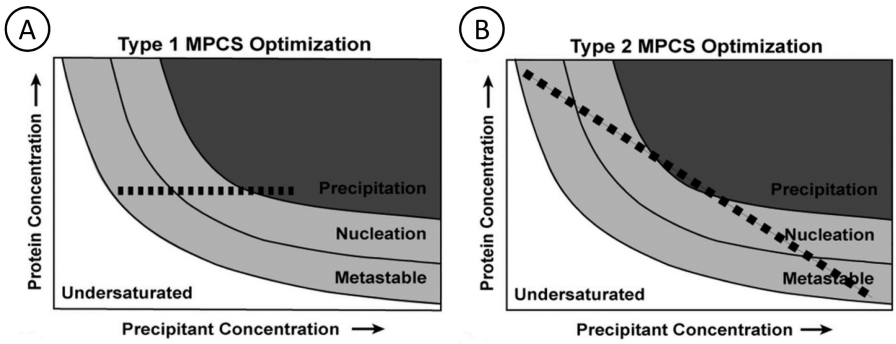

Figure 7: Protein crystallization phase diagrams indicating how crystallization phase space is interrogated in MPCS optimizations. (A) In Type 1 MPCS optimizations, the protein concentration is held constant while a gradient of precipitant concentration is generated over a series of droplets. (B) In Type 2 MPCS optimizations, the protein concentration begins high and slowly decreases as precipitant concentration starts low and increases slowly to generate a dynamic protein versus precipitant gradient over a series of droplets [Gerdts *et al.* 2010].

Beside the crystallization of nanocrystals, the MPCS can be adapted to study protein aggregation of e.g. αS and the influence of effectors. For the experiment, one channel is filled with native proteins (e.g. unfolded αS monomers). Another one is filled with effectors e.g. misfolded proteins, aggregates or even brain extracts from former

PD patients. The last component is buffer to create an ideal environment and to allow concentration adjustments. After mixing the components, the droplets can be observed by bright field, birefringence or UV imaging. This methods can be used to monitor the spreading of misfolded proteins among the native ones. Furthermore the aggregates can be analysed with cryo-EM after incubation.

2 Materials and Methods

Setups for the CZE and for the MPCS were assembled and the different instrumentations are described in detail. The operating softwares for each setup was programmed in LabVIEW.

Contents

2.1 Capillary Zone Electrophoresis

2.1.1 Setup Description

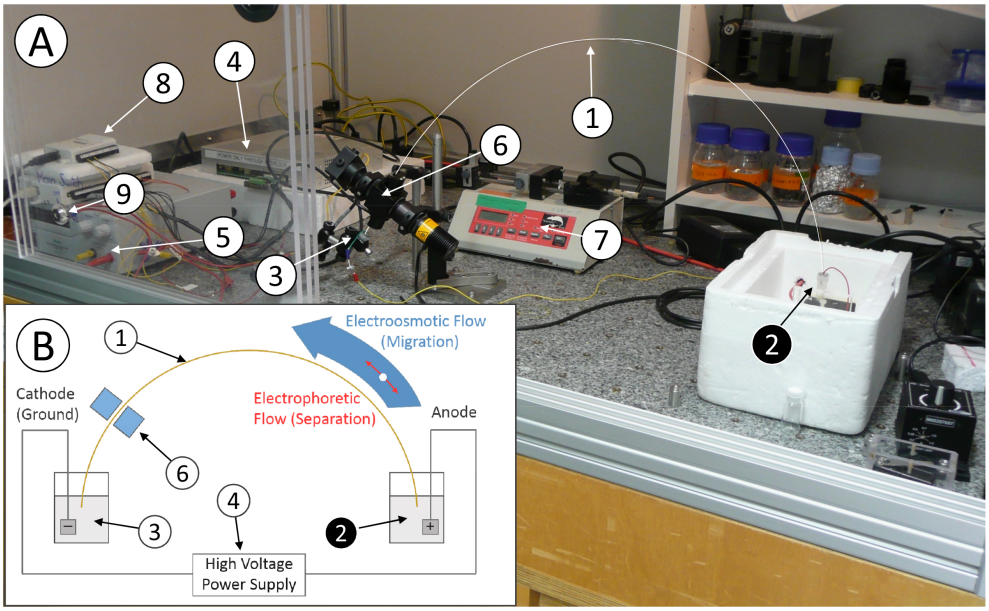

Figure 8: (A) CZE setup consisting of a capillary (1), two flasks with either an anode (2) or a cathode electrode (3) placed in it, a high voltage power supply (4) and its power source (5) as well as a capillary protein detector (CPD) (6). Furthermore a syringe pump (7) and USB data acquisition (DAQ) cards (8) are used. An interlock switch was built in for safety reasons (9). (B) Schematic drawing with the same labelling.

The CZE setup is seen in Figure 8. An extended light path capillary with an inner diameter of 75 µm (Figure 8.1, G1600-62332, Agilent Technologies) is placed with one end into a flask with the anode electrode dipped in (Figure 8.2) and the other end into one with a cathode (ground) electrode (Figure 8.3). The high voltages for the electrodes are delivered by a high voltage supply (Figure 8.4, KA-30R0.25, Matsusada Precision) with output voltages from 0 to 30 kV. A 24 V (I_{max} = 5 A) power supply (Figure 8.5, HCS-3202, Manson) is needed to operate the high voltage supply. A capillary protein detector (CPD) (Figure 8.6), whose setup will be explained later in detail, is placed near the anode end of the capillary to monitor the protein separation. All the hardware control, except the manual syringe pump, and the data acquisition are done by two USB data acquisition (DAQ) cards (Figure 8.8, NI USB-6211 and NI USB-6009, National Instruments). Furthermore a syringe (81062, Hamilton) is mounted onto a manual syringe pump (Figure 8.7, YA-12, indulab AG) is used to fill and flush the capillary. The used test proteins were lysozyme (A3711, Panreac AppliChem) and ribonuclease A (RNase A, A2760, Panreac AppliChem).

Capillary The fused silica capillary has an inner diameter of 75 µm and an effective length of 80 cm. It is externally coated with polyimide to increase the mechanical strength. It has an uncoated optical viewing window with an extended inner diameter of 200 µm (Figure 9). This extended light path called 'bubble-cell' increases the sensitivity of the capillary protein detector by a factor of 2.7. The shape of the extension guarantees a non turbulent flow and therefore prevent dispersions of the separated protein bands. Since risk of breaking the capillary is increased at this uncoated region, the capillary need to be handled carefully.

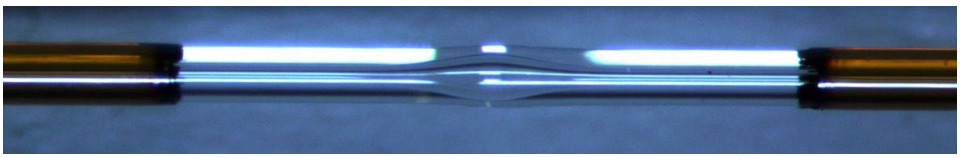

Figure 9: Optical viewing window of an extended light path capillary (ID = 75 µm) with the visible 'bubble cell' (ID = 200 µm)

Capillary Protein Detector (CPD) The used light source is a mounted high-power light-emitting diode (LED) (Figure 10.1, M280L3, Thorlabs), which emits incoherent light at a wavelength of 280 nm. This wavelength is ideal, since proteins (i.e. the amino acids tryptophan and tyrosine) absorb light of this energy [Edelhoch 1967]. The LED is controlled by an LED driver (LEDD1B, Thorlabs), whose maximum output current is set to 350 mA.

The light is then collimated by a spherical piano-convex lens (Figure 10.2, LA4280, Thorlabs). A lens with a very small diameter (Ø = 6 mm) and a short focal length (f = 10.0 mm) is used to capture most of the emitted light into a narrow light beam. The light beam has a high intensity concentrated on a small cross sectional area, which is crucial fo the sensitivity of the detector.

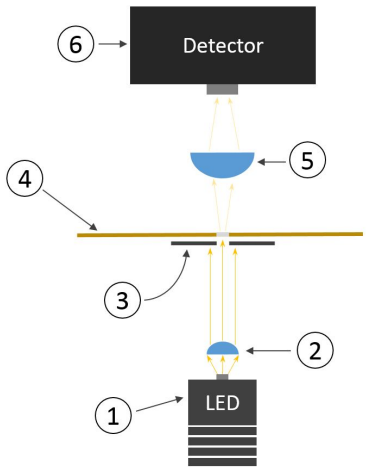

Figure 10: Schematic drawing of the CPD with a LED light source (1), a collimator lens (2), a slit aperture (3), an extended light path capillary (4), a focusing lens (5) and a GaP UV-Detector with a build-in amplifier(6).

Afterwards the light is projected onto a 50 µm slit aperture (Figure 10.3, S50R, Thorlabs), with a slit length of 3 mm. The optical viewing window of the capillary (Figure 9) is placed directly behind the slit, so that all the light passing through the slit travels through the capillary (Figure 10.4). The capillary is hold in place by two fiber clamps (SM1F1-250, Thorlabs) centered in a lens tube cube (SM1C6, Thorlabs). The alignement is done under a light microscope by orienting the slit parallel to the capillary. Then the fiber clamps are used to slightly adjust the centring of the capillary for a perfect alignment.

Behind the capillary, a spherical piano-convex lens (Figure 10.5, Ø = 0.5", f = 10.0 mm, LA4647, Thorlabs) focuses the light onto a gallium phosphide (GaP) UV-detector (Figure 10.6, PDA25K-EC, Thorlabs) which has a build-in amplifier and detects light between 150 - 550 nm. The lenses consist of uncoated fused silica in order to allow the light (λ = 280 nm) to pass through. The UV-absorption signal is read out by using a USB DAQ card (NI USB-6211, National Instruments) and LabVIEW was used to process and save the data. The detailed setup with all the used parts such as lens tubes, spacers and adapters is shown in Figure 11.

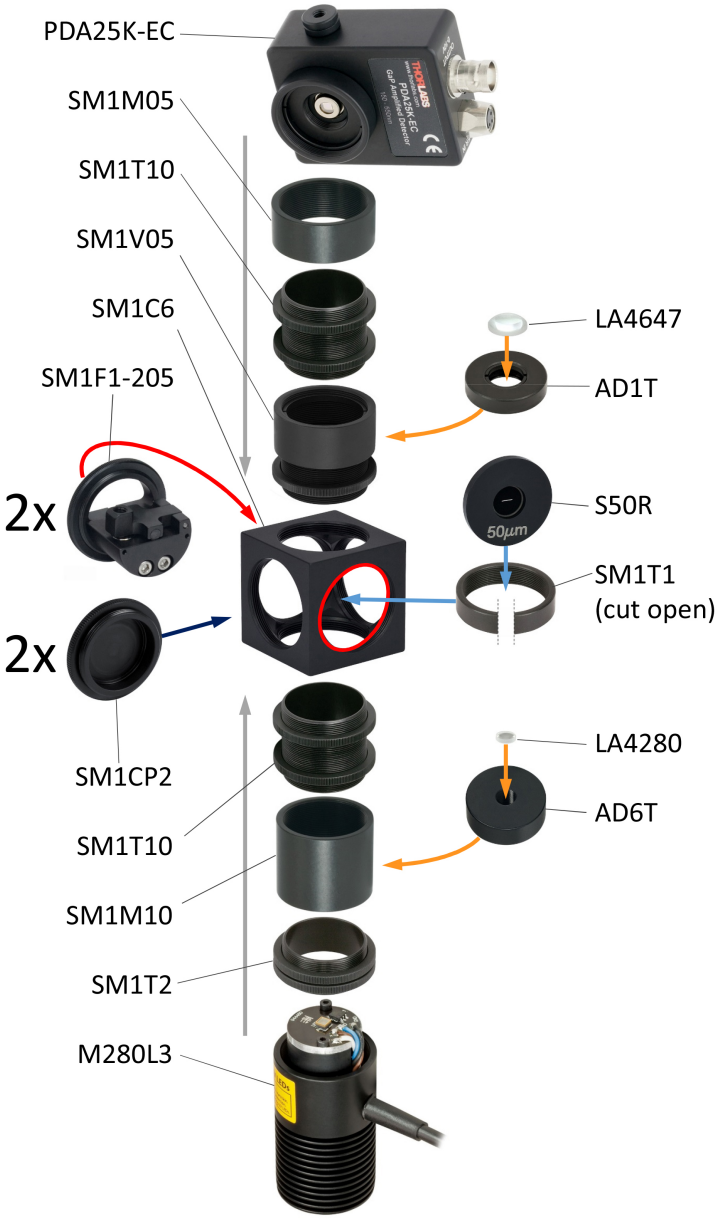

Figure 11: CPD setup. The slit aperture is mounted on a 0.3" lens tube, which is cut open to enable the insertion into the cube (blue arrows). Two fiber clamps are placed at the opposite ends of the cube (red arrow and circle). The lenses are mounted on top of adapters and placed into lens mounts (orange arrows). Everything is assembled (grey arrows). The remaining openings of the cube are closed by two caps (black arrows).

2.1.2 Hardware wiring

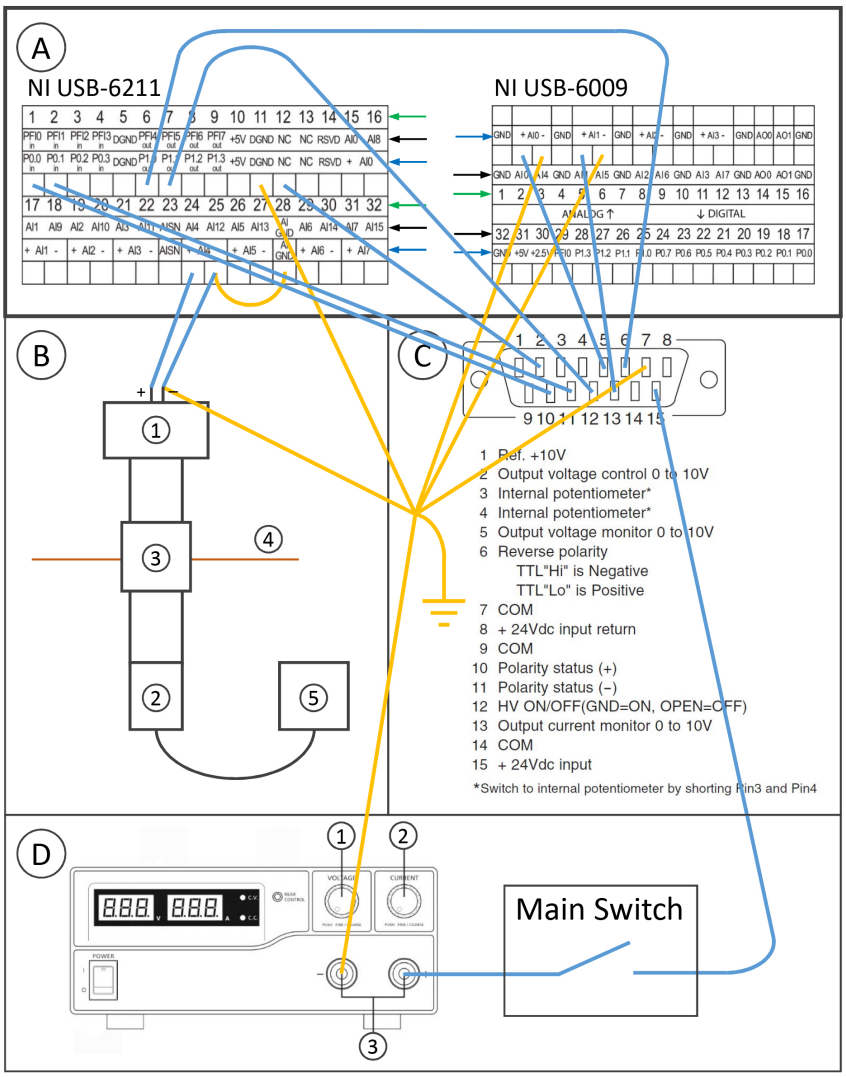

Figure 12: The wires connecting the hardware (blue lines) and wires connected to a common ground (yellow lines). The different parts are as follows. (A) DAQ cards with connectors either labelled by terminal name (green arrow), Single-Ended Signal Name (black arrow) or Differential Signal Name (blue arrow). (B) The CPD with a GaP detector (1), a LED (2), a Lens tube cube (3), a capillary (4) and a LED driver (5). (C) High voltage power supply. (D) 24V power source with Output Voltage Control (1), Output Current Control (2) and Aux. output terminal (3).

2.1.3 Experimental Procedure

Preconditioning of Capillary The capillary is first rinsed with 0.1 M NaOH for 10 minutes with a flow rate of 6 µL/min. When a new capillary is used, the flushing time extends to 20 minutes. Afterwards, the capillary is flushed for 5 minutes with distilled water and another 5 minutes with the running buffer, both with a flow rate of 6 µL/min). This guarantees that the pH returns to the buffer's pH level. The precondition is needed to uniformly charge the fused silica walls. In addition the capillary is cleaned. After the preconditioning step, the loose end of the capillary is placed into the cathode flask. A small volume is injected to get rid of bubbles. Then the other end is carefully disconnected from the syringe and placed into the anode flask. Be sure to always keep this end of the capillary under the height level of the other end, otherwise it is possible, that air is aspirated.

Sample Injection The sample is injected into the capillary by using the hydrostatic pressure. The anode end of the capillary is dipped into a sample flask and the flask is lifted up 50 cm for about 10 - 15 s (the other end of the capillary is still placed in the cathode flask). The volume of the injected sample can be measured by weighting the sample flask before and after the injection. It is very important to always inject a water droplet after the sample injection. This causes the sample droplet to be prefocused via isotachophoresis [Malá *et al.* 2013] before the separation starts, which increases the resolution and enables the formation of nicely separated bands.

Start experiment The high voltage (10 - 30 kV) is switched on. The current should increase to a steady level. When the EOF is already known, the migrating time of the protein can be estimated. If the current breaks down, the capillary is clogged. The capillary then needs to be flushed with the buffer and the sample has to be loaded again.

Post-experiment When the experiments are finished, the capillary is first rinsed with 0.1 M NaOH for a few minutes and then 5 minutes with distilled water. Before storing the capillary, blow-dry the capillary for about 5 minutes with N_2.

2.1.4 Software

The power supply control (Figure 13A) is used to control the high voltage and to monitor the current flow. After initializing the program, the voltage and the

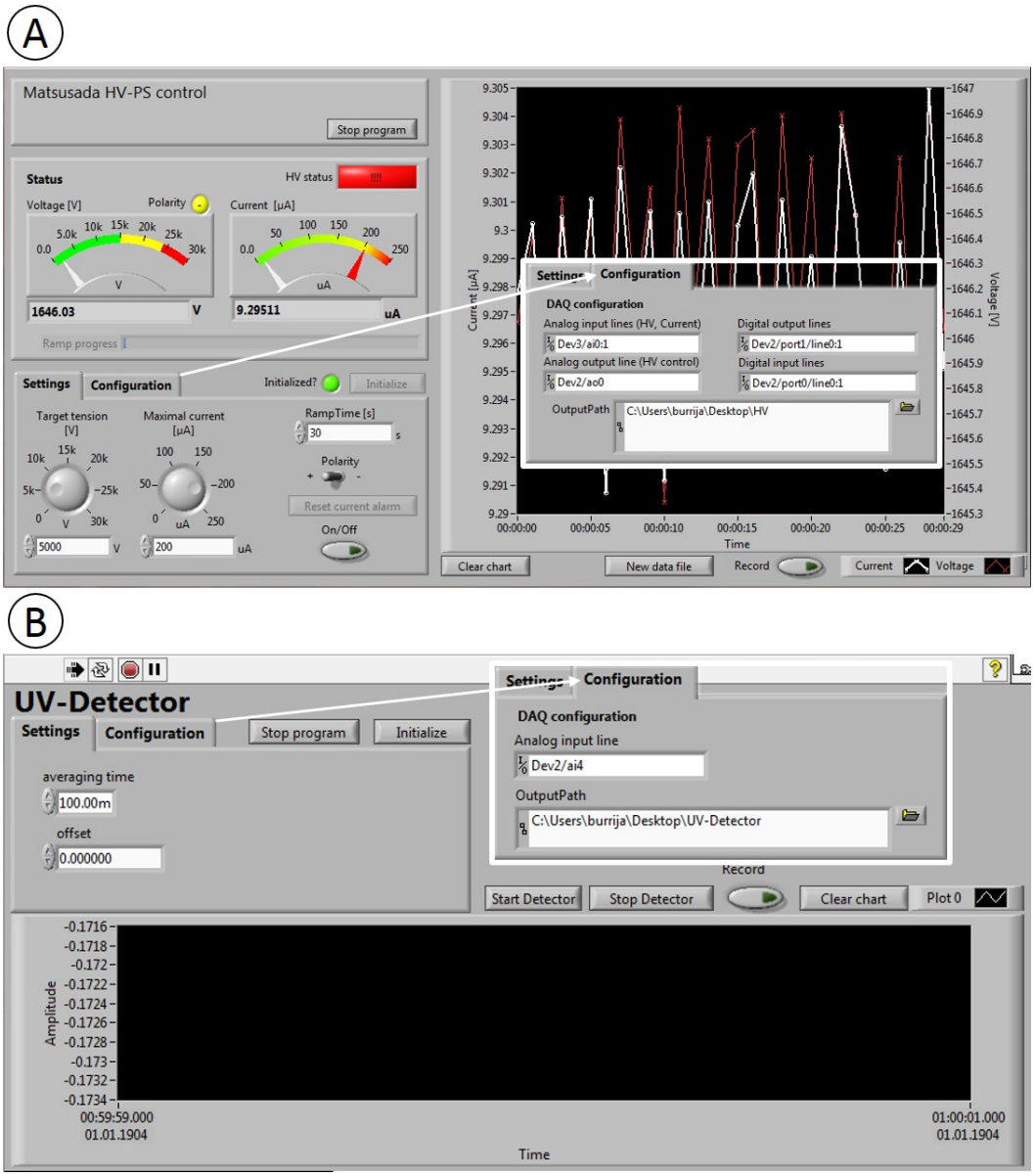

Figure 13: The user interfaces of the high voltage (A) and the CPD software (B).

maximum current can be adjusted in the settings. The time for the high voltage to start up is given by the ramp time. Once the voltage is started up, it can be altered without any delay. The ramp time can be circumvented by setting the starting voltage to 0 V and switch it on. After that, the voltage can be set immediately to any different level. The status bar monitors the real-time voltage and current

output. When the current exceeds the previously set maximum current, the current alarm is activated and the voltage is shut down. The record button is used to record the measurements. When multiple measurements are recorded, make sure to always create a new data file before starting the measurement. Assign the right lines of the DAQ cards according to the hardware wiring in the configuration panel. Furthermore, the output path for the data can be set.

The CPD software (Figure 13B) digitalizes the analogue voltage signal coming from the detector amplifier and shows it in a graph. After initializing, the detector can be started. The DAQ card line which is connected to the detector has to be set in the configuration panel. The averaging time and the offset of the signal can be adjusted in the settings panel. The data is saved at the given output path as a binary file. The binary file can be converted into a ASCII spreadsheet file using the ReadOutBinary.vi SubVI (Figure 14). There is also a combined software for the high voltage and CPD control, but it is more convenient to operate them separately. For the two programs to oparate simultaneously it is crucial, that the analog input lines of the two programs are on different DAQ cards.

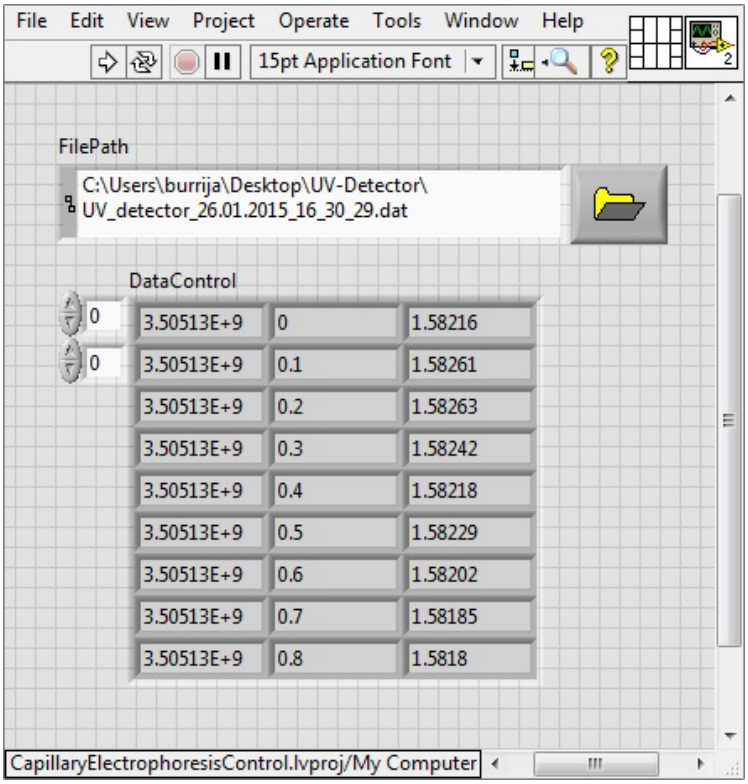

Figure 14: The binary files of the UV-detector can be converted into ASCII spreadsheet files by simply loading in the file path and running the VI.

2.2 Microcapillary Protein Crystallization System

2.2.1 Access of the Chip

The MPCS Crystal Card™ (EBS-400.2, Emerald BioSystems™) is mounted onto an home-made chip holder (Figure 15.1). Teflon tubes (Figure 15.2, 211921-10, BGB Analytik) are inserted into the corresponding holes in the chip holder. A flangeless connection is assured by a ferrule fitting (M-650X, MedChrom). The connection between the chip and the tubes are sealed using o-rings (FPM75, Hug). The Teflon tubes are fitted tightly to the syringes (Figure 15.3, 81062, Hamilton and 2624715, Innovative Labor Systeme GmbH) by a nut (JR-55050-10, Vici AG) and ferrule (JR-CFL-CB1KF, Vici AG) system. The syringes are mounted onto low pressure, high precision syringe pumps (Figure 15.4, neMESYS, cetoni GmbH). A camera (FOculus) is used to observe the droplet formation in the Crystal Card™.

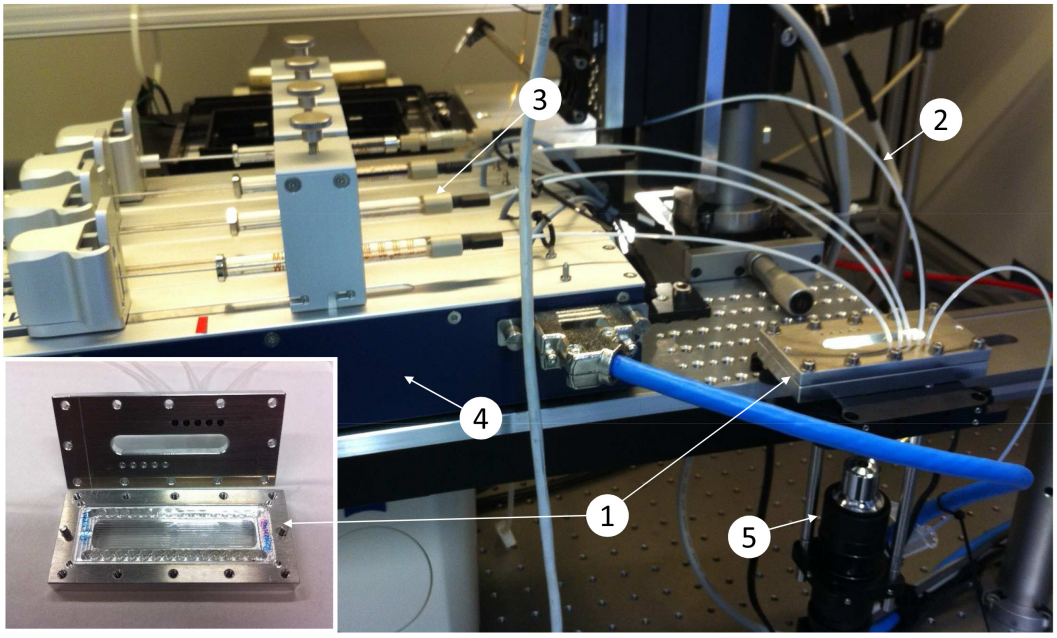

Figure 15: MPCS setup. The Crystal Card™ is placed into the chip holder (1), Teflon tubes (2) connect the chip holder with 100 µL syringes (3), which are mounted onto syringe pumps (4). The droplet formation is observed by a camera (5).

2.2.2 Experimental Procedure

1. Fill the syringes avoiding bubbles and mount them onto the syringe pumps and connect them with the Teflon tubes.
2. Start filling the Teflon tubes connected to the chip holder.
3. Remaining air bubbles are first flushed out of the Teflon tubes, before mounting the chip onto the chip holder. Fill bubble-free Teflon tubes right before the chip holder.
4. Close the chip holder by tightening the screws crosswise.
5. Fill the channels right up to the 3+1 mixer.
6. Press 'Generate Droplets' to start droplet formation with the concetration gradient. Sometimes the fluid flow back into one channels. This indicates, that there are still some air bubbles. Restart at step 3.

2.2.3 Software

In the neMESYS pump panel (Figure 16A) all the syringes can be activated separately by clicking on the green squares. The volume, which will be infused or withdrawn and the flow rates can be set individual for each syringe. The current flow rate and the dispensed volume can be observed. Furthermore the activated syringes can be emptied or filled. The inner diameter and the piston stroke of the activated syringes have to be set in the configuration panel (Figure 16B). Furthermore the syringe pumps can be initialized, calibrated or disconnected. For the droplet experiments, the constant flow rates (e.g. oil, protein) as well as the time step between the flow rate changes of the third component can be set. The droplet experiment is started by pressing the 'Generate Droplets' button in Figure 16A.

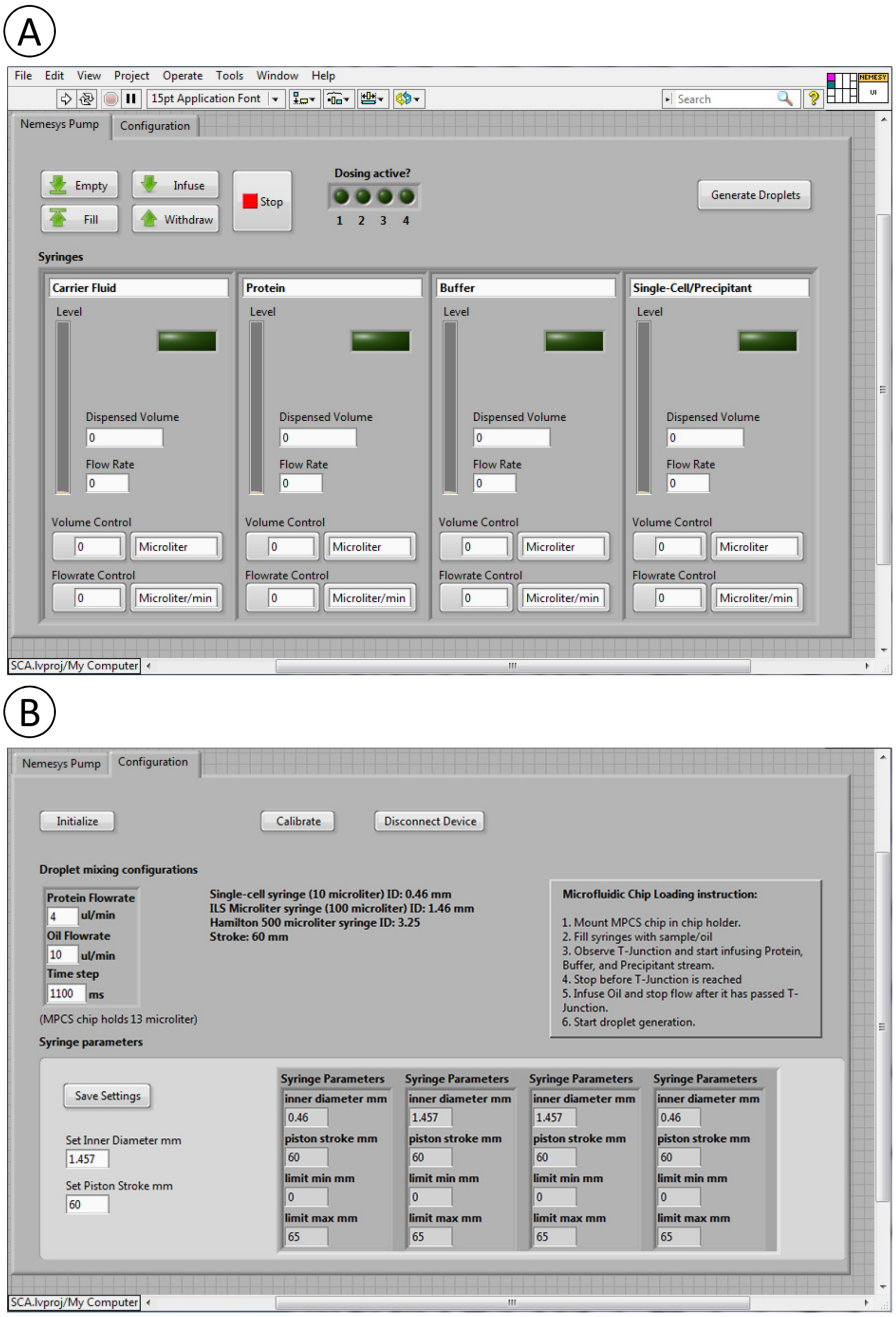

Figure 16: The user interface of the MPCS control. (A) In the experimental panel of the software, flow rates and volumes can be adjusted and infused or withdrawn. Furthermore the syringes can be emptied and filled. The droplet formation is started by pressing 'Generate Droplets'. (B) In the configuration panel, syringe parameters and the constant oil and protein solution flow rates are set. Furthermore a short operating instruction of the MPCS is given.

3 Results and Discussion

Different experiments were performed to test the CPD and the CZE setup. The MPCS, which was previously used to grow lysozyme crystals, was improved and experiments with RNase were made.

Contents

3.1 Detection Limit of the Capillary Protein Detector (CPD)

The CPD is tested by measuring different protein concentration. The capillary is connected to a syringe and filled with water. The end near the optical viewing window and therefore near the CPD is loose. The syringe pump is set to withdraw 5 µL/min and one after another the buffer (0.1 M NaAc pH 4.) and the lysozyme solutions (lysozyme in 0.1 M NaAc pH 4.6) were aspirated in through the loose end of the capillary. The solution droplets were separated by air bubbles so that they stay separated and dispersion is prevented. The absorption at $\lambda = 280$ nm (Figure 17) of the different droplets is continuously measured when they flow through the optical viewing window Figure 17.

There is an increased signal at the transition from water to the buffer solution although the buffer contains no protein which could absorb light. This is probably an effect of the shape of the optical viewing window ('bubble cell'), which acts as some kind of a lens. Therefore the diffraction indices influence how much of the light is focused onto the detector. This is supported by the fact, that the signal is only 0.14 V when the bubble cell is empty (filled with air). In this case, most of the light is diffracted away from the detector.

A closer look at the absorption of the last buffer droplet shows, that the right value is not directly achieved. In fact the signal first increases and then adjusts to the right level. This is most probably a result from some lysozyme still sticking to the wall. Furthermore, the different absorption values for water before and after the lysozyme droplets indicate a baseline shift. This baseline shift could be resulting

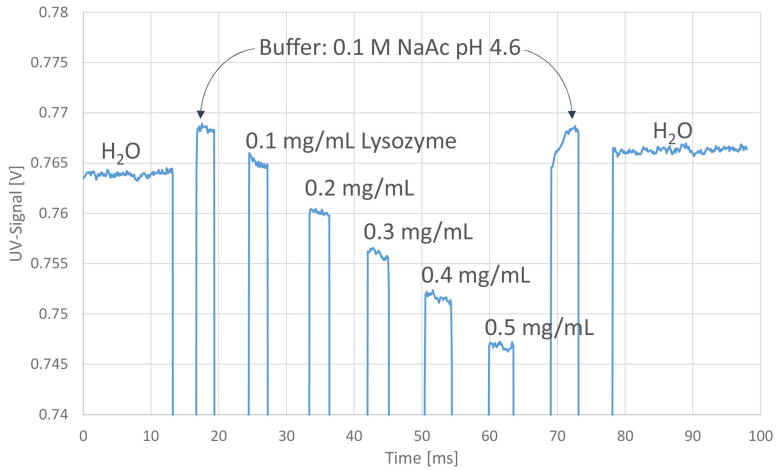

Figure 17: Absorption measurement of different fluid droplets with an increasing protein concentration gradient separated by air bubbles.

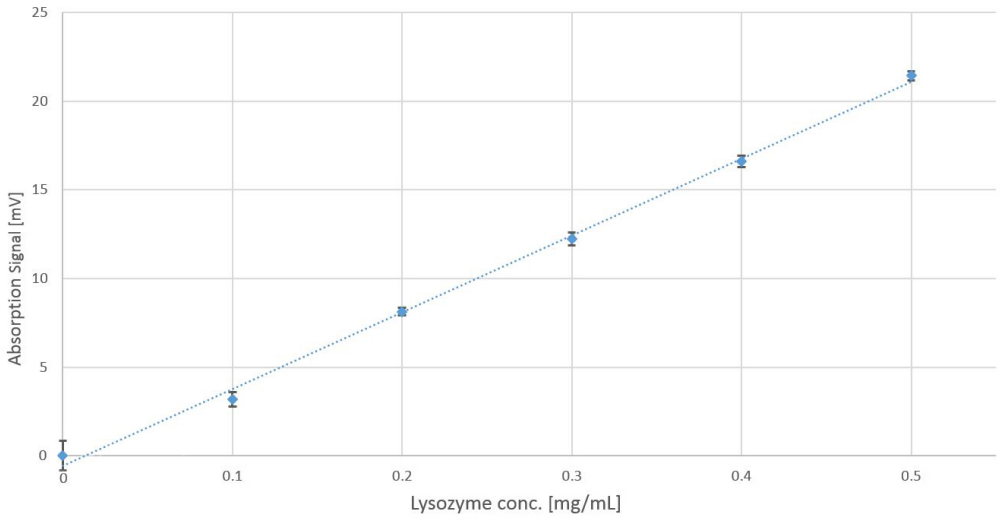

Figure 18: Absorption signal of different lysozyme concentration with standard derivations and a linearly fitted trendline.

from buffer film still sticking to the wall of the capillary. Baseline shifts should be prevented to get consistent high resolution results.

The UV-signals of the droplets in Figure 17 are used to determine the effective absorption of the lysozyme (Figure 18). The baseline is given by the UV-signal of the buffer and is subtracted from the original UV signal, to solely display the lysozyme absorption. A linear dependency between lysozyme concentration and

absorption is observed. The fitted function indicates an increased absorption signal of 4.33 mV for each concentration step of 0.1 mg/mL. It is said, that different signal have to be separated by three time the standard derivation to be distinguishable. Since the mean value of the standard derivation is 0.4 mV, it is estimated, that concentration differences of about 0.03 mg/mL can be distinguished.

3.2 Separation of Protein Mixture

3.2.1 Electroosmotic Flow

The EOF can be measured by injecting a neutral solvent into the capillary. In this particular experiment the used running buffer was 0.1 M K_2SO_4 in 50 mM HEPES at pH 7.4. The injected sample is a 1:1:1 solution of acetone, water and buffer. Because of the large current, the operating voltage was set to 10 kV.

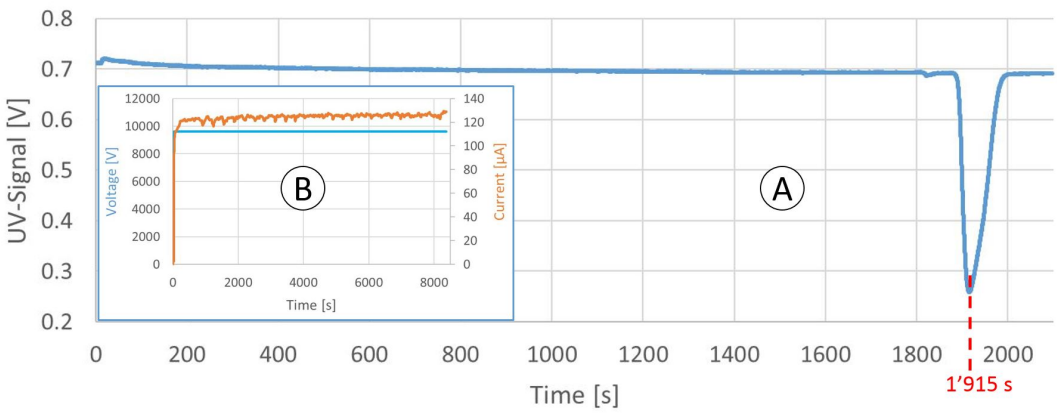

Figure 19: (A) The CZE absorption spectrum of acetone with the running buffer 0.1 M K_2SO_4 in 50 mM HEPES at pH 7.4. (B) The voltage is set to 10 kV with a corresponding current of about 125 - 130 µA.

The advantage of using acetone, is its maximum extinction coefficient at around λ = 280 nm (ϵ_{vapor} = 11.3 $M^{-1}cm^{-1}$ [Bayliss & McRae 1954]). The absorption peak of acetone is observed after a running time of 1'915 s (Figure 19A). The current needs some time to reach a constant value, but then is more less steady (Figure 19B).

With the observed t_{eff} =1'915 s = 31.9 min and the volume of the capillary (ID = 75 µm, L = 80 cm) $V_{capillary} = r^2\pi L$ = 3.53 µL given, the EOF can be calculated.

$$Flow\ rate = \dot{V} = V_{capillary}/t_{eff} = 0.11\ \mu L/min \tag{4}$$

The EOF is only linked to the running buffer and should not depend on the injected samples.

3.2.2 Lysozyme/RNase Mixture

A test sample consisting of 0.1 mg/mL lysozyme and 0.1 mg/mL ribonuclease A (RNase A) in running buffer was used to test the separation capabilities. The lysozyme (M=14.4 kDa, pI=11.35) and the RNase (M=13.7 kDa, pI=9.6) are of similar size and are both positively charged, since their isoelectric point is above the pH of the running buffer. Therefore one would expect a similar electrophoretic behaviour which complicates the separation of the two proteins. Different running buffer and additives were tested.

Phosphate Buffered Saline Buffer Phosphate buffered saline (PBS) was first used as the running buffer to separate the test solution. The reason for trying PBS is that PBS is widely used for biological systems, since it offers a physiological environment. Furthermore recent aggregation experiments with αS are made in PBS buffer. The high salt concentration only allows to apply a voltage of 10 kV (Figure 20B).

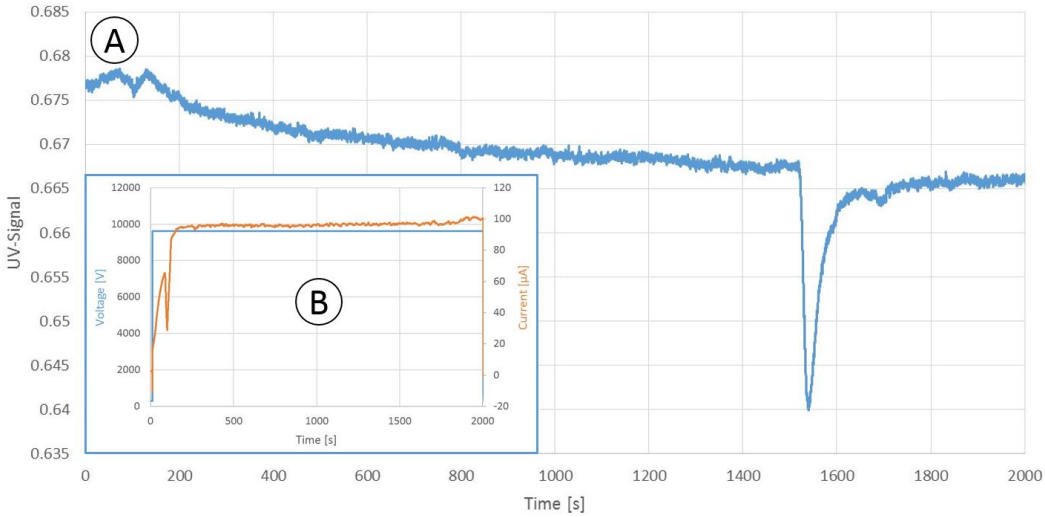

Figure 20: CZE separation of a Lysozyme/RNase mixture using PBS as the running buffer. (A) The UV-absorption spectrum and (B) the Voltage/Current Graph.

Unfortunately the absorption spectrum only shows one large peak (maybe an additional very small one on the right side). Therefore it can be concluded, that either

the proteins could not be separated or that most of one of the positively charged component is adsorbed to the negatively charged wall, which would decrease the amount of this component drastically.

HEPES Buffer with K_2SO_4 In this experiment the running buffer is 0.1 M K_2SO_4 in 50 mM HEPES buffer at pH 7.4. It has been shown that using K_2SO_4 is superior to NaCl and KCl, which are contained in PBS, since it prevents protein adsorptions to the wall [Bushey & Jorgenson 1989]. HEPES belongs to the Good's buffers [Good *et al.* 1966] which are zwitterionic buffers. Zwitterionic buffers are often used for CZE since they minimize the conductance of the liquid and therefore reduce the current.

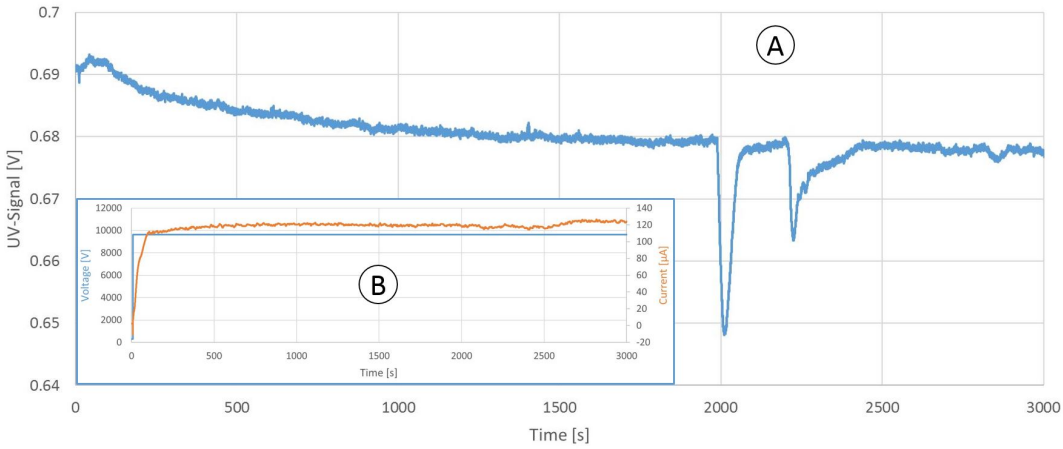

Figure 21: CZE separation of a Lysozyme/RNase mixture using 0.1 M K_2SO_4 in 50 mM HEPES buffer at pH 7.4 as the running buffer. (A) The UV-absorption spectrum and (B) the applied voltage and the corresponding current.

An overview of the CZE experiment is seen in Figure 21. A voltage of 10 kV was applied and the observed current stayed at a steady level after a short increase (Figure 21B). The CZE absorption spectrum shows two nicely separated bands (Figure 21A). For the analysis of the peaks, a closer look is needed (Figure 22). The two peaks have some fundamental differences. The earlier one is a single peak with a large absorption signal. The second one has a smaller absorption and two side peaks can be observed. After the peaks, the signal need some time to adjust again, resulting most probably from protein adsorption to the wall.

Lysozyme contains more of the absorbing amino acids (tryptophan and tyrosine) and have therefore a larger extinction coefficient $\epsilon_{1\%}$. Furthermore the used lysozyme has a purity of nearly 100%, whereas the RNase contains as well some traces of

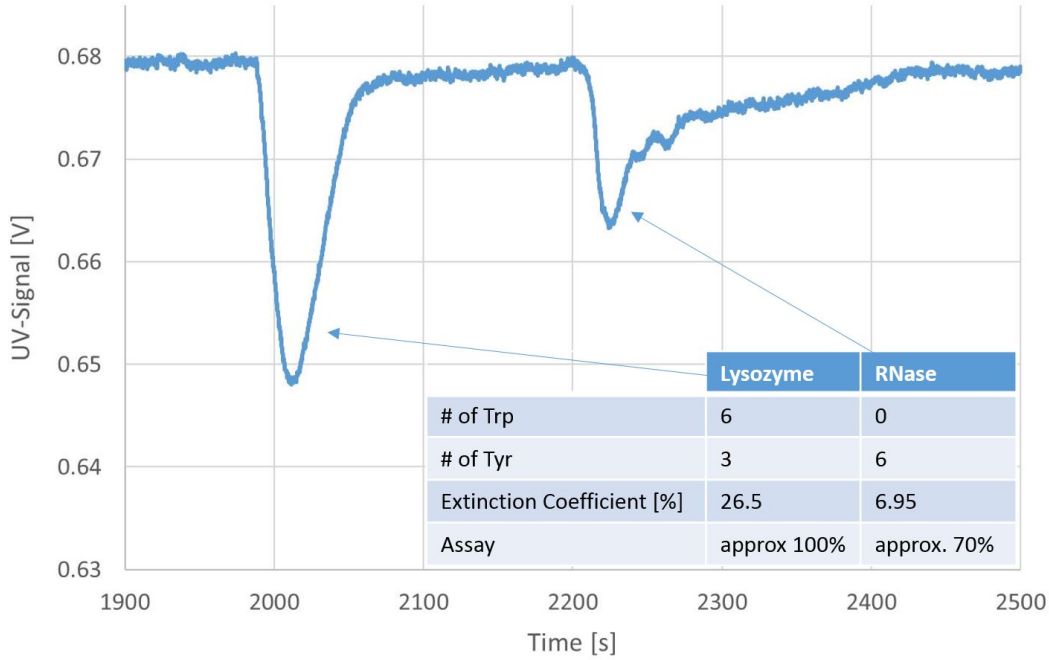

Figure 22: Lysozyme and RNase is assigned to the corresponding peaks regarding their properties.

DNases and proteases. Most probably, these impurities have similar properties than the RNase. Otherwise they would have been filtered out during purification. As a conclusion, the larger extinction coefficient and the high purity of lysozyme leads to a large, single peak, whereas the RNase has a smaller peak with some side peaks resulting form DNases and proteases. When all this is taken into account, the two proteins can definitely be assigned to each one of the peaks (Figure 22).

3.2.3 Cell Lysate

The next step is to look at a biological sample. For that purpose, Human Embryonic Kidney (HEK) cell are lysed using ultrasonic sound. The lysate was then injected into the CZE. Since the 0.1 M K_2SO_4 in 50 mM HEPES buffer at pH 7.4 worked quite well in the previous CZE, it was used again as the running buffer.

The voltage is set to 10 kV and the responding current shows the typical short increase onto a certain level (around 130 µA), where it stays more or less steady (Figure 23B). The absorption signal was much weaker than the ones using the test sample and no clear bands could be observed (Figure 23A). But a broadened signal with two higher peaks was found. The CZE absorption spectrum gives no clues on

the composition of the different parts of the separation. Therefore fractions of this volume need to be hand over onto different ex situ instruments, such as cryo-EM, to get a better insight in the separation process.

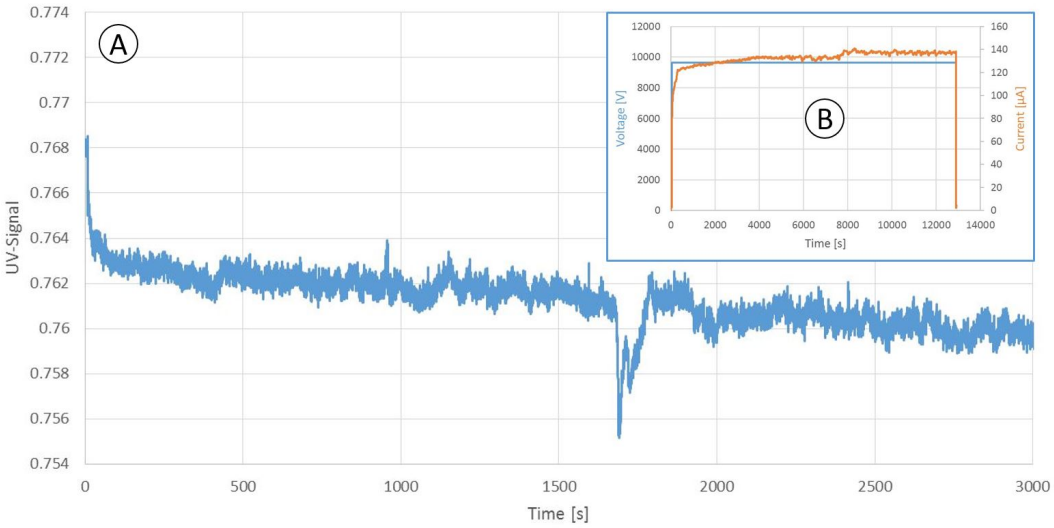

Figure 23: CZE separation of HEK cell lysate using 0.1 M K_2SO_4 in 50 mM HEPES buffer at pH 7.4 as the running buffer. (A) The UV-absorption spectrum and (B) the voltage and current.

3.3 Detector Problems

3.3.1 "Jumps"

One of the biggest problems with the detector is his "environmental" sensitivity. This leads to signal jumps between two discrete values (Figure 24). The actual signal is set between these two values. These jumps are much bigger then the normal noise and prevent to detect weak absorption signals. This effect always occurred at the end of the month. The rest of the month, the detector could be used without any problems except during December in which this jumps appeared even during the month.

It can be excluded that this disturbance is coming from the built-in amplifier, since the jumps are observed when the amplifier is turned off, as well as at the highest amplification (Figure 24). It can be determined, that the problem depends only on the detector since the signal coming into the detector was measured and checked. The jumps occurred as well, when the LED was turned off (Figure 24A). Possibly,

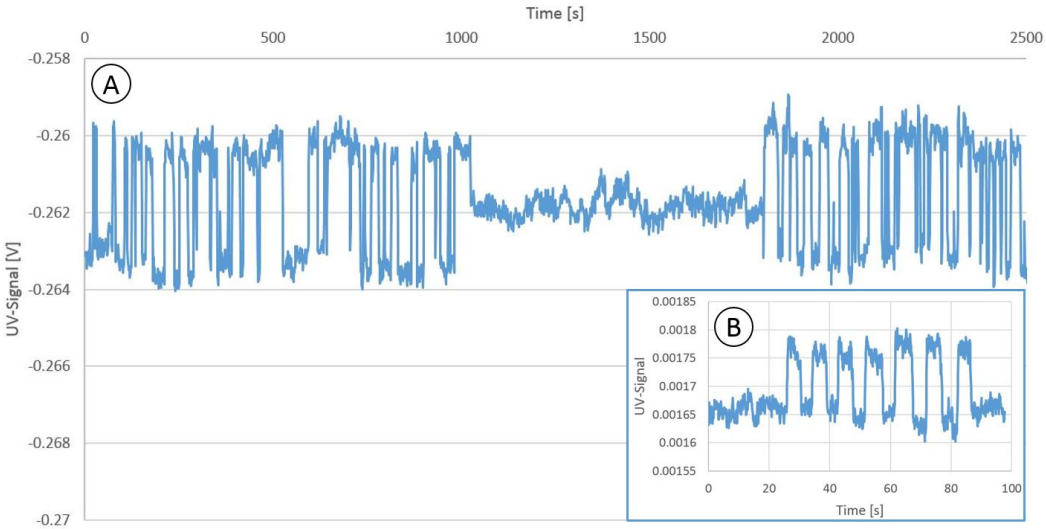

Figure 24: Signal jumps in the detector signal. (A) Two periods with jumps separated by a period with normal signals without any abnormalities. The amplification is set to 70 dzB and the LED is switched off. (C) The jumps are observed as well, when the amplification is turned off (0 dzB).

the jumps can be prevented using a lock-in amplifier or a detector of higher quality, but further experiments have to be done.

3.3.2 Warming Up

When the detector is switched on, the signal declines asymptotically until it reaches a steady value. Everytime the LED is set to a different value this effect is observed again. Therefore the detector and the LED have to be switched on for at least one hour before the experiments can be started.

3.3.3 Current Changes

The detector 'feels' intense current fluctuations. When the CZE is turned on the current increase until it reaches a more or less stable value. This change in current results in a little increased signal from the detector, which can be seen in all the CZE absorption spectra (Figure 19, 20, 21 and 23). The signal then returns asymptotically to the normal level. Since the current should be constant during the CZE experiment, this effect should not influence the detection of protein bands.

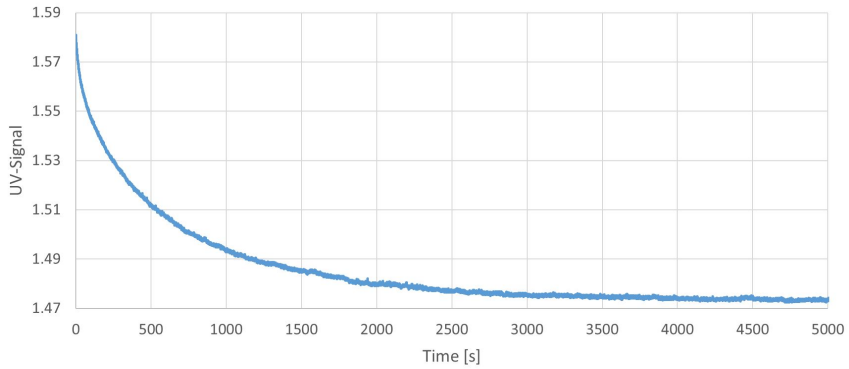

Figure 25: UV-Signal, after switching on the Detector and the LED, shows a exponential approximation towards the real signal.

3.4 RNase Crystals

It has been previously shown, that the MPCS can be used to grow lysozyme crystals [Burri 2014]. Unfortunately it was not possible to observe nanocrystals. One reason was the high symmetry of the lysozyme crystals. High symmetric crystals do not generate second harmonic generation (SHG) which is essential to be accessed by second order nonlinear imaging of chiral crystals (SONICC) [Kissick *et al.* 2011]. Therefore SONICC yield no signals of nanoparticles although it can detect crystals down to a scale of 90 nm [Kissick *et al.* 2011].

Therefore another attempt was done using fluorescence labelled RNase A instead of lysozyme. The fluorescence picture of the first trials looked promising. The crystal like structures of the bright field microscope lit up in the fluorescence images (Figure 26). It can not be concluded, if these structures are unordered aggregates or crystals. Unfortunately it was not possible to examine the exact same chips by SONICC since the chips tried out during incubation because of the volatile separation oil. Other chips were prepared with RNase for SONICC and confocal microscopy analyses. The observed chips showed no sign of crystals in the chip. Either there are no crystals in the chip or the crystals were two small to be properly located. This is especially a problem when SONICC is used. A precise coordination system of the different droplets in the channels is missing, furthermore the bright field microscope and the SONICC can not be operated simultaneously. In addition to the location in x,y-direction, it is also crucial that the SONICC observe the right plane in z-direction. This leads to a more or less blind search for nanocrystals.

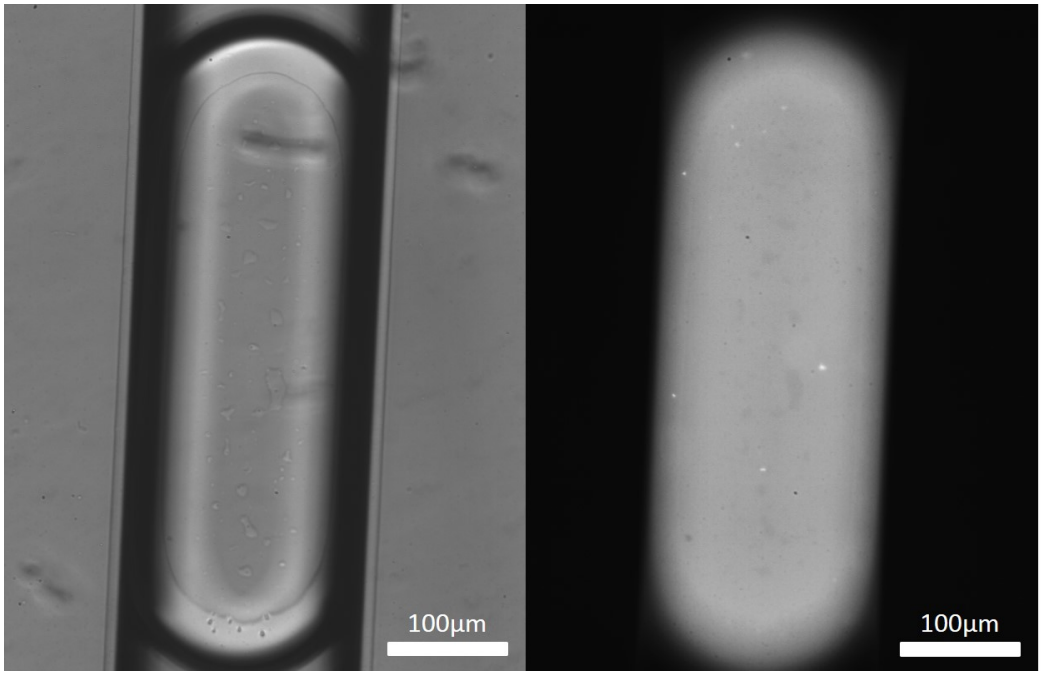

Figure 26: Bright field and fluorescence image of a droplet. RNase crystals are visible as bright spots.

3.5 MPCS Disadvantages

The idea of merging multiple channels and separate them with an oily phase to form lots of small experiments is a good approach. But there are some disadvantage of the chip which makes it inevitable to design a new chip. First, after the incubation and crystallization, it is difficult to access the crystals. Attempts to extract the nanocrystals by cleaving of the protecting membrane or by simply pumping the droplet out of the outlet, resulted either in a fast evaporation of the fluid or in a merging of almost all droplets into one. Furthermore the in situ analysis using birefringence, which would be a simple and effective method to detect protein crystals, is restricted by the slightly birefringent chip material. Another problem is the difficulty to establish a coordinate system for the different droplets in the channel, which is essential for a lot of analysis instruments, such as SONICC.

Until now, we were not able to recycle the chip, which would lead to great costs on the long run. One problem which has been solved is the clogging of the chip, which previously even started at the beginning of the experiment. This clogging disturbed or completely prevented the formation of droplets. The solution was to simply replace the previous used oil FC-40 with a more viscose oil (mcs-oil 04).

4 Conclusions and Outlook

A CPD was designed and assembled which can detect small protein concentrations of 0.1 mg/mL. Furthermore a setup for CZE was built up and established. The setup was used to successfully separate a test sample consisting of lysozyme and RNase A by using 0.1 M K_2SO_4 in 50mM HEPES buffer at pH 7.4 as the running buffer and a voltage of 10 kV. The resulting bands were assigned to each protein. Furthermore a method to measure the EOF was presented and successfully realised. First attempts were made to separate cell lysates from HEK cells.

The setup is far from perfect and there are some improvement which has to be made in the near future. First a higher quality detector has to be built in the CPD. Hopefully, this prevents the uncontrollable signal jumps and decreases the sensitivity for current changes. Furthermore the DAQ cards, which are only meant for method development, should be replaced by professional control and data acquisition cards. The quality of the CZE can be increased by using a capillary with an inner diameter of 25 µm instead of the 75 µm one. This would decrease the current by a factor of 9 and allows higher voltages to be applied. Protein adsorption can be reduced by shortening the capillary. Since this would again increase the current, an optimal ratio between capillary length and diameter has to be found.

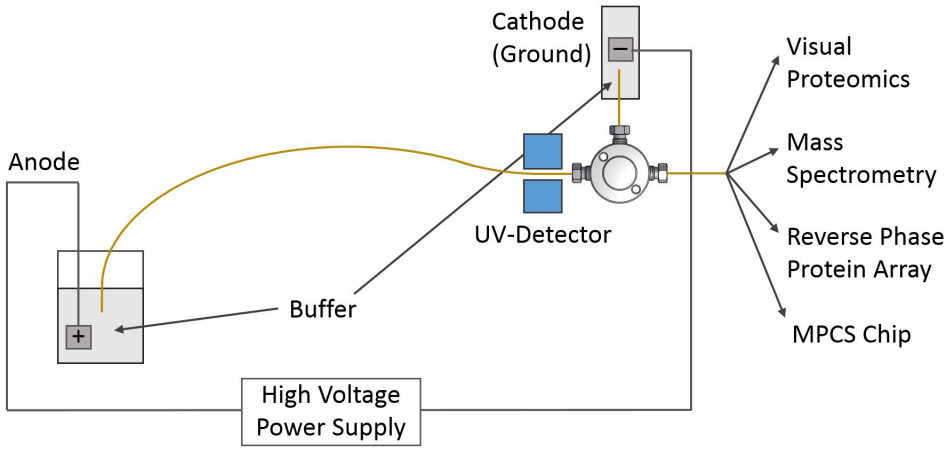

Figure 27: A schematic drawing of an improved CZE setup where the sample can be pumped out after separation.

In the present setup the separated band are difficult to access. After the separation, the cathode flask has to be removed, otherwise the proteins would flow into the flask. A much more practical setup is seen in Figure 27, a similar one was already presented in [Zhou & Johnston 2004]. This improved CZE has a T-connector at the cathode end of the capillary. A completely sealed buffer flask with a glued-in cathode

electrode is connected to the T-connector, separated by a semipermeable membrane. This allows only the electrolytes but no bigger particles to pass through. After the separation the voltage is simply turned off and the anode flask is elevated. The hydrodynamic pressure pumps the separated bands out of the capillary and onto the next analysis instrument, e.g. cryo-EM or into the MPCS for further processing.

It has been shown, that the MPCS can be used to apply a fine concentration gradient and therefore tune the crystallization conditions. The droplet formation works reliable with an uncomplicated handling. Unfortunately there are too many disadvantages when it comes to access the grown crystals. It has not been possible to specifically extract a selected crystal. Further disadvantages are first, that the amount of different component which can be mixed is limited to three and second, that there is a large dead volume in the Teflon tubes connecting the chip to the syringes. A more open design to easily inject and extract the different components would be helpful. Furthermore, this would simplify the integration into the aspired microfluidic pipeline (Figure 1).

This thesis presents some preliminary work to realize a microfluidic system for protein separation, aggregation and nanocrystallization. A method to separate complicated protein mixtures and a system to promote and monitor aggregation and nanocrystallization were presented. These two instrumentations have to be combined to form the microfluidic system. For that purpose the individual instrumentations have to be improved to solve problems regarding handover and liquid handling between them.

Acknowledgments

I would like to thank Stefan Arnold for the great supervision, advice and support building up my setup. I further thank Thomas Braun for the coordination of the project, great supervision and for helping with LabVIEW issues. Special thanks to Henning Stahlberg for the opportunity to do my master's thesis at the C-CINA. Furthermore, I thank Paul Baumgartner for his help with the dialysis instruments. I thank all members of Thomas Braun's subgroup (Benjamin Bircher, Andrej Bieri, Roger Krenger, Dominic Giss, Rosmarie Sütterlin, Cedric Leu, Stefan Albiez and Claudio Schmidli) for interesting and informative discussion during coffee breaks and after-work pints and for helping me improving my foosball skills.

References

[Aguzzi & Calella 2009] Adriano Aguzzi and Anna Maria Calella. *Prions: protein aggregation and infectious diseases.* Physiological reviews, vol. 89, pages 1105–1152, 2009. (Cited on page 1.)

[Angot *et al.* 2012] Elodie Angot, Jennifer A Steiner, Carla M Tomé, Peter Ekström, Bengt Mattsson, Anders Björklund and Patrik Brundin. *Alpha-synuclein cell-to-cell transfer and seeding in grafted dopaminergic neurons in vivo.* PLoS ONE, vol. 7, no. 6, pages 23–27, 2012. (Cited on page 2.)

[Bayliss & McRae 1954] Noel S Bayliss and Eion G McRae. *Solvent effects in the spectra of acetone, crotonaldehyde, nitromethane and nitrobenzene.* The Journal of Physical Chemistry, vol. 58, no. 5, pages 1006–1011, 1954. (Cited on page 27.)

[Bogan 2013] Michael J. Bogan. *X-ray free electron lasers motivate bioanalytical characterization of protein nanocrystals: Serial femtosecond crystallography.* Analytical Chemistry, vol. 85, pages 3464–3471, 2013. (Cited on page 3.)

[Bousset *et al.* 2013] Luc Bousset, Laura Pieri, Gemma Ruiz-Arlandis, Julia Gath, Poul Henning Jensen, Birgit Habenstein, Karine Madiona, Vincent Olieric, Anja Böckmann, Beat H Meier and Ronald Melki. *Structural and functional characterization of two alpha-synuclein strains.* Nature communications, vol. 4, page 2575, 2013. (Cited on page 3.)

[Burré *et al.* 2010] Jacqueline Burré, Manu Sharma, Theodoros Tsetsenis, Vladimir Buchman, Mark R Etherton and Thomas C Südhof. *Alpha-synuclein promotes SNARE-complex assembly in vivo and in vitro.* Science (New York, N.Y.), vol. 329, pages 1663–1667, 2010. (Cited on page 2.)

[Burri 2014] Jan Burri. *Two-Phase Microfluidics for Protein Nanocrystallization.* Project Thesis, 2014. (Cited on pages 3 and 33.)

[Bushey & Jorgenson 1989] Michelle M Bushey and James W Jorgenson. *Capillary electrophoresis of proteins in buffers containing high concentrations of zwitterionic salts.* Journal of Chromatography, vol. 480, pages 301–310, 1989. (Cited on page 29.)

[Chapman *et al.* 2011] Henry N Chapman, Petra Fromme, Anton Barty, Thomas a White, Richard a Kirian, Andrew Aquila, Mark S Hunter, Joachim Schulz, Daniel P DePonte, Uwe Weierstall, R Bruce Doak, Filipe R N C Maia, Andrew V Martin, Ilme Schlichting, Lukas Lomb, Nicola Coppola, Robert L Shoeman, Sascha W Epp, Robert Hartmann, Daniel Rolles, Artem Rudenko,

Lutz Foucar, Nils Kimmel, Georg Weidenspointner, Peter Holl, Mengning Liang, Miriam Barthelmess, Carl Caleman, Sébastien Boutet, Michael J Bogan, Jacek Krzywinski, Christoph Bostedt, Saša Bajt, Lars Gumprecht, Benedikt Rudek, Benjamin Erk, Carlo Schmidt, André Hömke, Christian Reich, Daniel Pietschner, Lothar Strüder, Günter Hauser, Hubert Gorke, Joachim Ullrich, Sven Herrmann, Gerhard Schaller, Florian Schopper, Heike Soltau, Kai-Uwe Kühnel, Marc Messerschmidt, John D Bozek, Stefan P Hau-Riege, Matthias Frank, Christina Y Hampton, Raymond G Sierra, Dmitri Starodub, Garth J Williams, Janos Hajdu, Nicusor Timneanu, M Marvin Seibert, Jakob Andreasson, Andrea Rocker, Olof Jönsson, Martin Svenda, Stephan Stern, Karol Nass, Robert Andritschke, Claus-Dieter Schröter, Faton Krasniqi, Mario Bott, Kevin E Schmidt, Xiaoyu Wang, Ingo Grotjohann, James M Holton, Thomas R M Barends, Richard Neutze, Stefano Marchesini, Raimund Fromme, Sebastian Schorb, Daniela Rupp, Marcus Adolph, Tais Gorkhover, Inger Andersson, Helmut Hirsemann, Guillaume Potdevin, Heinz Graafsma, Björn Nilsson and John C H Spence. *Femtosecond X-ray protein nanocrystallography.* Nature, vol. 470, pages 73–77, 2011. (Cited on page 3.)

[Costanzo & Zurzolo 2013] Maddalena Costanzo and Chiara Zurzolo. *The cell biology of prion-like spread of protein aggregates: mechanisms and implication in neurodegeneration.* The Biochemical journal, vol. 452, pages 1–17, 2013. (Cited on pages 1 and 2.)

[Doerr 2011] Allison Doerr. *Diffraction before destruction.* Nature methods, vol. 8, no. 4, page 283, 2011. (Cited on page 4.)

[Dolník 1994] Vladislav Dolník. *Capillary gel electrophoresis.* Journal of Microcolumn Separations, vol. 6, no. 4, pages 315–330, 1994. (Cited on page 5.)

[Edelhoch 1967] H Edelhoch. *Spectroscopic determination of tryptophan and tyrosine in proteins.* Biochemistry, vol. 6, pages 1948–1954, 1967. (Cited on page 14.)

[Frost & Diamond 2010] Bess Frost and Marc I Diamond. *Prion-like mechanisms in neurodegenerative diseases.* Nature reviews. Neuroscience, vol. 11, pages 155–159, 2010. (Cited on page 2.)

[Gerdts *et al.* 2010] Cory J Gerdts, Glenn L Stahl, Alberto Napuli, Bart Staker, Jan Abendroth, Thomas E Edwards, Peter Myler, Wesley Van Voorhis, Peter Nollert and Lance J Stewart. *Nanovolume optimization of protein crystal growth using the microcapillary protein crystallization system.* Journal of Applied Crystallography, vol. 43, pages 1078–1083, 2010. (Cited on page 11.)

[Goedert 2001] Michel Goedert. *Alpha-synuclein and neurodegenerative diseases.* Nature reviews. Neuroscience, vol. 2, pages 492–501, 2001. (Cited on page 2.)

[Good *et al.* 1966] Norman E Good, G Douglas Winget, Wilhelmina Winter, Thomas N Connolly, Seikichi Izawa and Raizada M M Sing. *Hydrogen ion buffers for bifological Research.* Biochemistry, vol. 5, no. 2, pages 467–477, 1966. (Cited on page 29.)

[Guo *et al.* 2013] Jing L Guo, Dustin J Covell, Joshua P Daniels, Michiyo Iba, Anna Stieber, Bin Zhang, Dawn M Riddle, Linda K Kwong, Yan Xu, John Q Trojanowski and Virginia M Y Lee. *XDistinct α-synuclein strains differentially promote tau inclusions in neurons.* Cell, vol. 154, no. 1, pages 103–117, 2013. (Cited on page 3.)

[Hansen *et al.* 2011] Christian Hansen, Elodie Angot, Ann-Louise Bergström, Jennifer A Steiner, Laura Pieri, Gesine Paul, Tiago F Outeiro, Ronald Melki, Pekka Kallunki, Karina Fog, Jia-Yi Li and Patrik Brundin. *α-Synuclein propagates from mouse brain to grafted dopaminergic neurons and seeds aggregation in cultured human cells.* The Journal of Clinical Investigation, vol. 121, no. 2, pages 715–725, 2011. (Cited on page 2.)

[Ironside *et al.* 2005] James W Ironside, Diane L Ritchie and Mark W Head. *Phenotypic variability in human prion diseases.* Neuropathology and applied neurobiology, vol. 31, pages 565–579, 2005. (Cited on page 3.)

[Jorgenson & Lukacs 1983] James W Jorgenson and Krynn D Lukacs. *Capillary zone electrophoresis.* Science (New York, N.Y.), vol. 222, pages 266–272, 1983. (Cited on page 4.)

[Kissick *et al.* 2011] David J Kissick, Debbie Wanapun and Garth J Simpson. *Second-order nonlinear optical imaging of chiral crystals.* Annual review of analytical chemistry (Palo Alto, Calif.), vol. 4, pages 419–437, 2011. (Cited on page 33.)

[Kühlbrandt & Williams 1999] Werner Kühlbrandt and Karen A Williams. *Analysis of macromolecular structure and dynamics by electron cryo-microscopy.* Current opinion in chemical biology, vol. 3, pages 537–543, 1999. (Cited on page 4.)

[Malá *et al.* 2013] Zdena Malá, Petr Gebauer and Petr Boček. *Recent progress in analytical capillary isotachophoresis.* Electrophoresis, vol. 34, pages 19–28, 2013. (Cited on pages 5 and 18.)

[Nederlof *et al.* 2013] Igor Nederlof, Yao Wang Li, Marin Van Heel and Jan Pieter Abrahams. *Imaging protein three-dimensional nanocrystals with cryo-EM.*

Acta Crystallographica Section D: Biological Crystallography, vol. 69, pages 852–859, 2013. (Cited on page 4.)

[Pedersen & Heegaard 2013] Jeppe T Pedersen and Niels H H Heegaard. *Analysis of protein aggregation in neurodegenerative disease.* Analytical Chemistry, 2013. (Cited on page 4.)

[Pedersen *et al.* 2011] Jeppe T Pedersen, Jesper Ø stergaard, Noemi Rozlosnik, Bente Gammelgaard and Niels H H Heegaard. *Cu(II) mediates kinetically distinct, non-amyloidogenic aggregation of amyloid-β peptides.* Journal of Biological Chemistry, vol. 286, no. 30, pages 26952–26963, 2011. (Cited on page 4.)

[Rodriguez-Diaz *et al.* 1997] Roberto Rodriguez-Diaz, Tim Wehr and Mingde Zhu. *Capillary isoelectric focusing.* Electrophoresis, vol. 18, no. 12-13, pages 2134–2144, 1997. (Cited on page 5.)

[Shi *et al.* 2013] Dan Shi, Brent L. Nannenga, Matthew G. Iadanza and Tamir Gonen. *Three-dimensional electron crystallography of protein microcrystals.* eLife, vol. 2013, pages 1–17, 2013. (Cited on page 4.)

[Spillantini *et al.* 1997] Maria G Spillantini, Marie L Schmidt, Virginia M-Y Lee, John Q Trojanowski, Ross Jakes and Michel Goedert. *Alpha-synuclein in Lewy bodies.* Nature, vol. 388, pages 839–840, 1997. (Cited on page 2.)

[Sunde *et al.* 1997] Margaret Sunde, Louise C Serpell, Mark Bartlam, Paul E Fraser, Mark B Pepys and Colin C Blake. *Common core structure of amyloid fibrils by synchrotron X-ray diffraction.* Journal of molecular biology, vol. 273, pages 729–739, 1997. (Cited on pages 1 and 2.)

[Vilar *et al.* 2008] Marçal Vilar, Hui-Ting Chou, Thorsten Lührs, Samir K Maji, Dominique Riek-Loher, Rene Verel, Gerard Manning, Henning Stahlberg and Roland Riek. *The fold of alpha-synuclein fibrils.* Proceedings of the National Academy of Sciences of the United States of America, vol. 105, no. 25, pages 8637–8642, 2008. (Cited on page 2.)

[Volles *et al.* 2001] Michael J Volles, Seung-Jae Lee, Jean-Christophe Rochet, Mark D Shtilerman, Tomas T Ding, Jeffrey C Kessler and Peter T Lansbury. *Vesicle permeabilization by protofibrillar alpha-synuclein: implications for the pathogenesis and treatment of Parkinson's disease.* Biochemistry, vol. 40, pages 7812–7819, 2001. (Cited on page 3.)

[Waxman & Giasson 2010] Elisa A Waxman and Benoit I Giasson. *A novel, high-efficiency cellular model of fibrillar α-synuclein inclusions and the examination of mutations that inhibit amyloid formation.* Journal of Neurochemistry,

vol. 113, pages 374–388, 2010. (Cited on page 2.)

[Waxman & Giasson 2011] Elisa A Waxman and Benoit I Giasson. *Induction of intracellular tau aggregation is promoted by α-synuclein seeds and provides novel insights into the hyperphosphorylation of tau.* The Journal of neuroscience : the official journal of the Society for Neuroscience, vol. 31, no. 21, pages 7604–7618, 2011. (Cited on page 3.)

[Weinreb *et al.* 1996] Paul H Weinreb, Weiguo Zhen, Anna W Poon, Kelly A Conway and Peter T Lansbury. *NACP, a protein implicated in Alzheimer's disease and learning, is natively unfolded.* Biochemistry, vol. 35, no. 43, pages 13709–13715, 1996. (Cited on page 2.)

[Yonetani *et al.* 2009] Motokuni Yonetani, Takashi Nonaka, Masami Masuda, Yuki Inukai, Takayuki Oikawa, Shin Ichi Hisanaga and Masato Hasegawa. *Conversion of wild-type α-synuclein into mutant-type fibrils and its propagation in the presence of A30P mutant.* Journal of Biological Chemistry, vol. 284, no. 12, pages 7940–7950, 2009. (Cited on page 3.)

[Zhou & Johnston 2004] Feng Zhou and Murray V Johnston. *Protein characterization by on-line capillary isoelectric focusing, reversed-phase liquid chromatography, and mass spectrometry.* Analytical Chemistry, vol. 76, no. 10, pages 2734–2740, 2004. (Cited on page 35.)

[Zhou 2008] Z Hong Zhou. *Towards atomic resolution structural determination by single-particle cryo-electron microscopy.* Current Opinion in Structural Biology, vol. 18, pages 218–228, 2008. (Cited on page 4.)

Additional information

List of abbreviations

αS	α-Synuclein
AD	Alzheimer disease
Aβ	Amyloid-β
CE	Capillary electrophoresis
CPD	Capillary protein detector
Cryo-EM	Electron cryomicroscope
CZE	Capillary zone electrophoresis
DAQ	Data acquisition
DED	Direct electron detection
EOF	Electroosmotic flow
GaP	Gallium phosphide
HD	Huntingon's Disease
HEK	Human embryonic kidney
HEPES	4-(2-hydroxyethyl)-1-piperazineethanesulfonic acid
Htt	Huntingtin
ID	Inner diameter
LED	Light-emitting diode
MicroED	Micro-electron-diffraction
MPCS	Microcapillary protein crystallization system
PBS	Phosphate buffered saline
PD	Parkinson's disease
pI	Isoelectric point
PMD	Protein misfolding disorders
PrP^{C}	Normal prion protein conformer
$PrP^{S}C$	Pathogenic prion protein conformer
RNase	Ribonuclease
SHG	Second harmonic generation
SONICC	Second order nonlinear imaging of chiral crystals
UV	Ultraviolet
XFEL	X-Ray Free-Electron Laser

List of Figures

List of Tables